JCB Journal of Cell Biology

ARTICLE

Telomerase treatment prevents lung profibrotic pathologies associated with physiological aging

Sergio Piñeiro-Hermida[1], Chiara Autilio[2], Paula Martínez[1], Fátima Bosch[3], Jesús Pérez-Gil[2], and Maria A. Blasco[1]

Short/dysfunctional telomeres are at the origin of idiopathic pulmonary fibrosis (IPF) in patients mutant for telomere maintenance genes. However, it remains unknown whether physiological aging leads to short telomeres in the lung, thus leading to IPF with aging. Here, we find that physiological aging in wild-type mice leads to telomere shortening and a reduced proliferative potential of alveolar type II cells and club cells, increased cellular senescence and DNA damage, increased fibroblast activation and collagen deposits, and impaired lung biophysics, suggestive of a fibrosis-like pathology. Treatment of both wild-type and telomerase-deficient mice with telomerase gene therapy prevented the onset of lung profibrotic pathologies. These findings suggest that short telomeres associated with physiological aging are at the origin of IPF and that a potential treatment for IPF based on telomerase activation would be of interest not only for patients with telomerase mutations but also for sporadic cases of IPF associated with physiological aging.

Introduction

Telomeres are protective structures at the ends of eukaryotic chromosomes that are essential for chromosome stability (Blackburn, 2001). In mammals, telomeric DNA consists of TTAGGG repeats bound by a six-protein complex termed "shelterin" (Liu et al., 2004; de Lange, 2005). Telomeres shorten due to the incomplete replication of DNA ends with each cell division, a phenomenon known as the "end-replication" problem (Watson, 1972; Olovnikov, 1973). Telomere shortening can be compensated through the de novo addition of telomeric repeats onto chromosome ends by telomerase, a reverse transcription composed of a catalytic subunit (TERT) and an RNA component (Terc) used as a template for telomere elongation (Greider and Blackburn, 1985). Critically short telomeres with aging are considered one of primary hallmarks of aging, since they can trigger other hallmarks of aging, such as genomic instability, cellular senescence, and apoptosis, mitochondrial dysfunction and loss of the regenerative capacity of tissues (Blasco, 2005; Blackburn et al., 2006; López-Otín et al., 2013). In the case of the lungs, aging causes a progressive impairment of lung function, including structural and immunological alterations that can impair the respiratory function and increase the risk of lung diseases (Lowery et al., 2013; Brandenberger and Mühlfeld, 2017). Indeed, aging is the main risk factor for developing chronic lung diseases, such as chronic obstructive pulmonary disease, lung cancer, and idiopathic pulmonary fibrosis (IPF; López-Otín et al., 2013; Meiners et al., 2015).

IPF affects ∼3 million people worldwide with a median survival time from diagnosis of 2–4 yr (Martinez et al., 2017; Richeldi et al., 2017; Raghu et al., 2018). As the major risk factor for IPF is age (Raghu et al., 2011; Faner et al., 2012; Selman and Pardo, 2014), its global incidence is predicted to increase in association with the worldwide phenomenon of demographic aging (Ley and Collard, 2013). In agreement with IPF being an age-associated disease, IPF patients present most of the hallmarks of aging including abnormal shortening of telomeres, genomic instability, mitochondrial dysfunction, increased oxidative stress, and senescence (Meiners et al., 2015; Selman and Pardo, 2014; Alder et al., 2008; Demopoulos et al., 2002; Bueno et al., 2015; Korfei et al., 2013).

Interestingly, between 8% and 15% of familial IPF cases are associated with mutations in telomerase or in telomere-protective proteins (Alder et al., 2008; Armanios et al., 2007; Tsakiri et al., 2007). In agreement with defects in telomere maintenance and accelerated telomere shortening being at the origin of these familial IPF cases, these patients show abnormally short telomeres (Alder et al., 2008; Armanios et al., 2007). Mutations in telomerase genes have been observed in 1–3% of sporadic cases of pulmonary fibrosis (Tsang et al., 2012;

[1]Telomeres and Telomerase Group, Molecular Oncology Program, Spanish National Cancer Centre, Madrid, Spain; [2]Department of Biochemistry and Molecular Biology, Research Institute "Hospital 12 de Octubre (imas12)," Complutense University, Madrid, Spain; [3]Center of Animal Biotechnology and Gene Therapy, Department of Biochemistry and Molecular Biology, School of Veterinary Medicine, Universitat Autònoma de Barcelona, Bellaterra, Spain.

Correspondence to Maria A. Blasco: mblasco@cnio.es.

Armanios and Blackburn, 2012; Armanios, 2013). Even in the absence of telomerase mutations, IPF patients are reported to have shorter telomeres than healthy individuals (Alder et al., 2008). Moreover, genome-wide association studies revealed that single nucleotide polymorphisms within the *Tert* gene increase the risk of lung fibrosis (Fingerlin et al., 2013; Codd et al., 2013). Thus, mutations in telomere maintenance genes are associated with the clinical manifestations of IPF (Alder et al., 2008; Armanios et al., 2007; Tsakiri et al., 2007; Fingerlin et al., 2013; Cronkhite et al., 2008; Chibbar et al., 2010) and other respiratory pathologies (Snetselaar et al., 2015; Stanley et al., 2015).

Short telomeres have been previously shown by us and others to impair stem cell function and tissue regeneration (Martínez and Blasco, 2011; Flores et al., 2005; Sharpless and DePinho, 2007). In the case of the lung, stem cell and progenitor compartments include bronchial SCGB1A1$^+$ club cells and SFTPC (surfactant protein C)$^+$ alveolar type II (ATII) cells (Rawlins et al., 2009; Kotton and Morrisey, 2014; Hogan et al., 2014). In the past, we showed that induction of telomere dysfunction specifically in ATII cells was sufficient to induce progressive and lethal pulmonary fibrosis in mice, demonstrating that dysfunctional telomeres ATII cells are at the origin of IPF (Povedano et al., 2015). We further demonstrated that the presence of short telomeres in lung cells triggered IPF in telomerase-deficient mice upon treatment with a low dose of the lung-damaging agent bleomycin, which did not induce fibrosis in wild-type mice. Interestingly, treatment with a telomerase gene therapy that activated telomerase in the lungs was sufficient to stop the progression of fibrosis in these mice (Povedano et al., 2018). Together, evidence from human patients and mouse models with short telomeres indicates that short/dysfunctional telomeres are at the origin of fibrosis.

However, it remains unknown whether physiological aging also leads to short telomeres in the lung and whether this increases the risk of IPF with aging. To address this, here we study telomere length and lung phenotypes both in wild-type and telomerase-deficient mice with increasing age. Furthermore, we address whether telomerase gene therapy could delay or prevent lung profibrotic phenotypes associated with physiological aging in wild-type and telomerase-deficient mice.

Results

Physiological aging leads to decreased ATII and club cells in the lungs of wild-type mice, and this is anticipated in telomerase-deficient mice

We first set out to address whether physiological aging in wild-type mice leads to lung pathologies. To this end, we performed a full characterization of mouse lungs at different ages (5, 8–9, 42–49, and 92–125 wk of age) in both wild-type and third-generation (G3) telomerase-deficient mice with short telomeres (Blasco et al., 1997) as a control for lung pathologies associated with accelerated telomere shortening (Fig. 1, A and B). We could obtain very old (92–125 wk) *Tert*$^{+/+}$ mice, but not G3 *Tert*$^{-/-}$ mice, owing to the fact that the latter have a shortened life span (Herrera et al., 1999a). First, we measured telomere length in the alveolar parenchyma and bronchi by performing an immuno–telomere quantitative FISH (Q-FISH) to measure telomere fluorescence intensity and the prosurfactant protein C and CC10 antibodies as markers for ATII and club cells, respectively. Immuno–telomere Q-FISH was performed on lung sections from both *Tert*$^{+/+}$ and G3 *Tert*$^{-/-}$ mice at different ages to measure telomeres in ATII and club cells with aging (Povedano et al., 2018; Canela et al., 2007; Flores et al., 2008). We determined both mean telomere fluorescence (mean telomere spot intensity) as an indication of the mean telomere length and the percentage of short telomeres corresponding to the 20th percentile of the telomere fluorescence intensity values of controls (5-wk-old *Tert*$^{+/+}$ mice). We found a gradual decrease in mean telomere fluorescence in ATII and club cells with increasing age in the lungs of *Tert*$^{+/+}$ mice (Fig. 1, C, D, and G). Interestingly, this decrease in mean telomere fluorescence in ATII and club cells was already detectable at young age in G3 *Tert*$^{-/-}$ compared with age-matched *Tert*$^{+/+}$ mice, and very old *Tert*$^{+/+}$ mice (92–125 wk) showed low telomere fluorescence similar to that of young 5-wk-old G3 *Tert*$^{-/-}$ mice (Fig. 1, C, D, and F). Also, the percentage of short telomeres in ATII and club cells was progressively increased with increasing age in *Tert*$^{+/+}$ mice and was already elevated in G3 *Tert*$^{-/-}$ mice at young ages compared with age-matched *Tert*$^{+/+}$ mice (Fig. 1, E and G). Together, these results demonstrate telomere shortening with age in the lungs of wild-type mice, reaching at old ages values similar to those of young G3 *Tert*$^{-/-}$ mice.

Next, we set out to determine whether telomere shortening with aging in *Tert*$^{+/+}$ mice lead to defects in the lung homeostasis. To this end, we quantified different lung cell types previously shown to be important for lung regeneration, such as ATII cells (positive for the surfactant protein C–SFTPC marker) and club cells (positive for the secretoglobin 1A1-SCGB1A1 marker; Giangreco et al., 2002; Rock et al., 2011; Guha et al., 2012; Desai et al., 2014). We found that physiological aging leads to a progressive decrease both in the proportion of SFTPC-positive ATII cells relative to the total number of alveolar cells and in the number of SCGBA1-positive club cells per epithelium length both in wild-type and G3 *Tert*$^{-/-}$ mice (Fig. 1, C, H, and I). Again, G3 *Tert*$^{-/-}$ mice already showed this reduction at young ages compared with age-matched *Tert*$^{+/+}$ mice, and at 42–49 wk, G3 *Tert*$^{-/-}$ mice showed a reduction in ATII cells and club cells that was equivalent to very old (92–125-wk-old) *Tert*$^{+/+}$ mice (Fig. 1, C, H, and I).

Aging leads to fibroblast activation and collagen deposits in wild-type lungs and this is anticipated in telomerase-deficient lungs

One of the phenotypes associated with lung degenerative pathologies is the presence of fibrosis. Thus, we next set out to explore the presence of profibrotic phenotypes in both *Tert*$^{+/+}$ and G3 *Tert*$^{-/-}$ mice associated with physiological aging. We found that both *Tert*$^{+/+}$ and G3 *Tert*$^{-/-}$ mice showed a progressive increment with age in the expression of vimentin, a marker of fibroblasts in the alveolar parenchyma (Fig. 2, A and B). At 42–49 wk of age, G3 *Tert*$^{-/-}$ mice showed a significantly higher percentage of vimentin-positive area per high-power field (HPF;

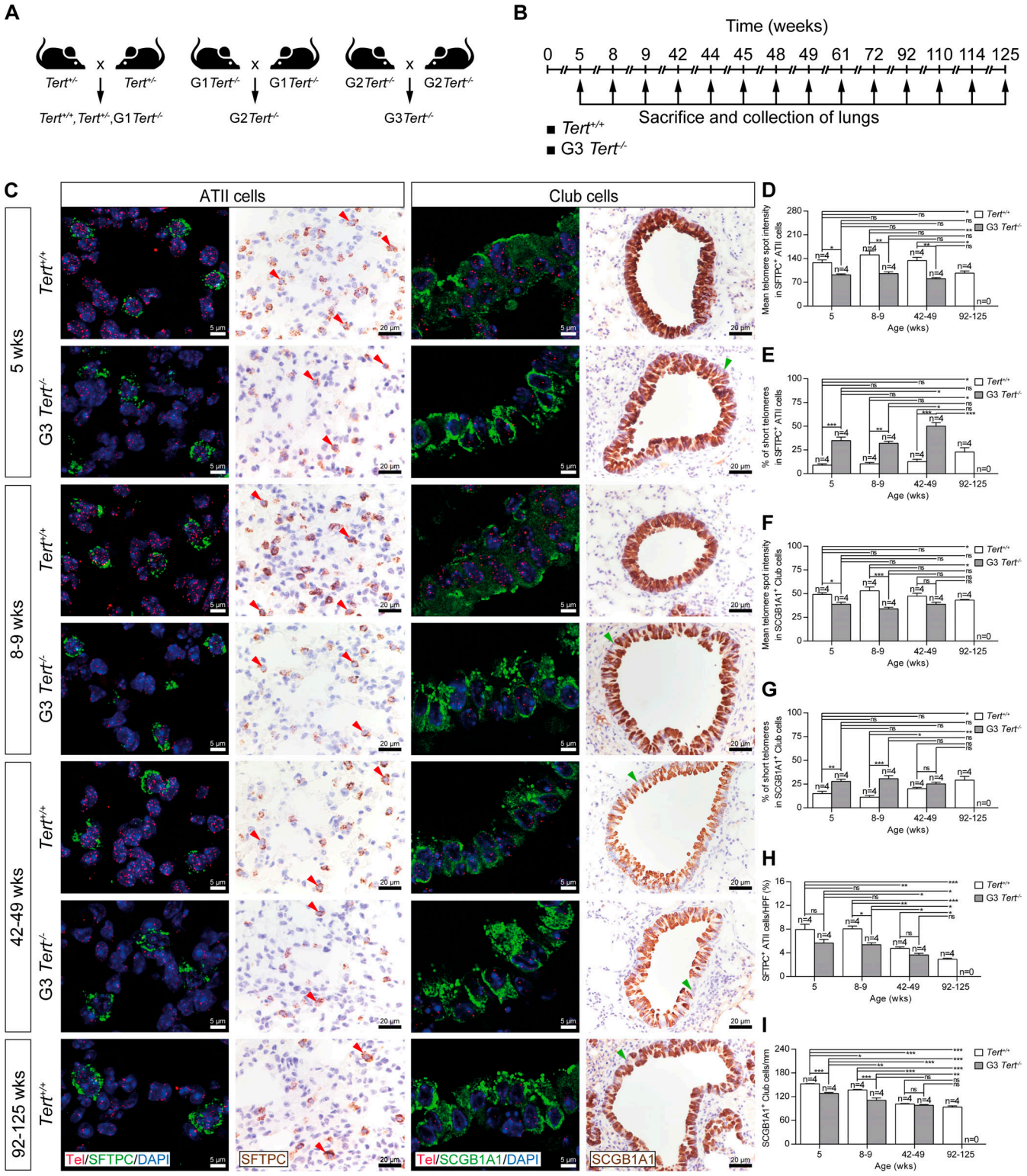

Figure 1. **Telomerase deficiency and natural aging in the mouse lung leads to telomere shortening and reduction in the number of ATII and club cells.** **(A and B)** Generation of *Tert*$^{+/+}$ and G3 *Tert*$^{-/-}$ mice and scheme of lung tissue harvesting. **(A)** Heterozygous *Tert*$^{+/-}$ mice were crossed to obtain *Tert*$^{+/+}$ and G1 *Tert*$^{-/-}$ mice, and successive crosses between G1 *Tert*$^{-/-}$ and then G2 *Tert*$^{-/-}$ mice were made to generate G3 *Tert*$^{-/-}$ mice. **(B)** Scheme of sacrifice and collection of lungs from *Tert*$^{+/+}$ and G3 *Tert*$^{-/-}$ mice at different time points. **(C)** Representative images showing a Q-FISH for telomere spot fluorescence in ATII and club cells (Cy3Tel probe [red], SFTPC- and SCGB1A1-positive cells [green]) and nuclei stained with DAPI (blue; left and center right), SFTPC (brown, red arrowheads; center left), and SCGB1A1 (brown, green arrowheads; right) immunostainings in lung sections from *Tert*$^{+/+}$ and G3 *Tert*$^{-/-}$ at different time points. **(D–I)** Quantification of mean telomere fluorescence (mean spot intensity; D and F), percentage of short telomeres in ATII and club cells corresponding to the 20th percentile of the fluorescence intensity values of controls (5-wk-old *Tert*$^{+/+}$ mice; E and G), and SFTPC-positive ATII cells (%) and SCGB1A1-positive club cells per epithelium length (millimeters; H and I). Quantifications were performed on five different alveolar areas or bronchi in a random way. Data are

expressed as mean ± SEM (*n* = 4 animals per group). *, P < 0.05; **, P < 0.01; ***, P < 0.001 (Shapiro–Wilk, Kruskal–Wallis, and Dunn–Sidak multiple comparison test). ns, not significant.

40× field) than age-matched *Tert*$^{+/+}$ mice and similar to those of very old (92–125-wk-old) *Tert*$^{+/+}$ mice (Fig. 2, A and B), suggesting anticipation of this phenotype in the absence of telomerase activity. Next, we studied fibroblast activation by analyzing the peribronchial expression of the smooth muscle actin (SMA) marker. We found that the percentage of

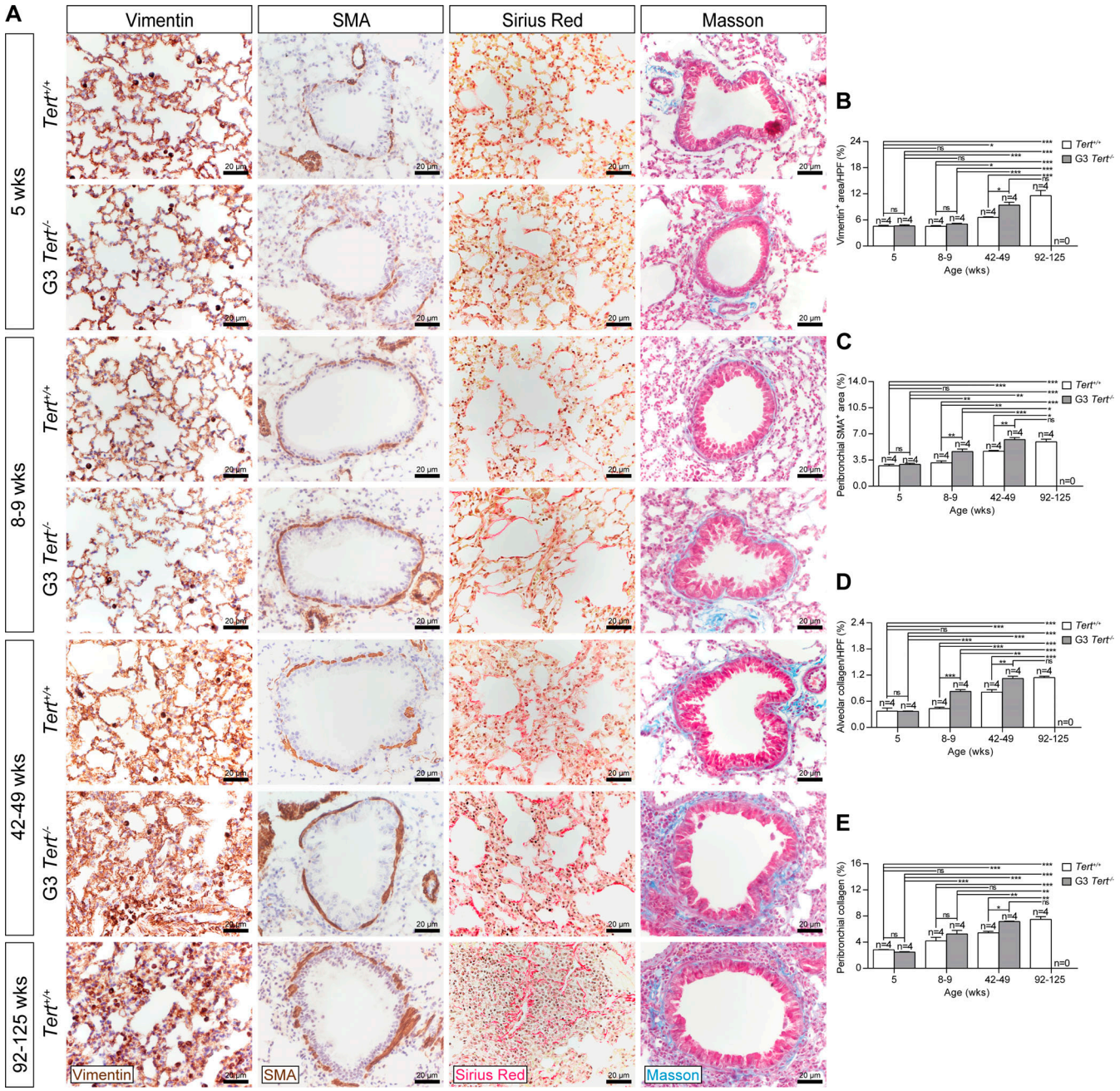

Figure 2. **Premature aging by accelerated telomere shortening and natural aging in the mouse lung result in increased fibroblast presence and activation and collagen deposition. (A)** Representative images showing vimentin (brown; left) and SMA (brown; center left) immunostainings and Sirius Red (red; center right) and Masson (blue; right) stainings in lung sections from *Tert*$^{+/+}$ and G3 *Tert*$^{-/-}$ mice at different time points. **(B–E)** Quantification of vimentin (fibroblast marker)–positive area per HPF (%; B), peribronchial SMA (fibroblast activation marker) –positive area (%; C), alveolar collagen content per HPF (%; D), and peribronchial collagen content (%; E). Quantifications were performed on five different alveolar areas or bronchi in a random way. Data are expressed as mean ± SEM (*n* = 4 animals per group). *, P < 0.05; **, P < 0.01; ***, P < 0.001 (Shapiro–Wilk, Kruskal–Wallis, and Dunn–Sidak multiple comparison test). ns, not significant.

peribronchial SMA-positive area gradually increased with age in *Tert*$^{+/+}$ and G3 *Tert*$^{-/-}$ mice, with G3 *Tert*$^{-/-}$ mice showing significantly more SMA positivity at 8–9 and 42–49 wk of age compared with age-matched *Tert*$^{+/+}$ mice (Fig. 2, A and C). Again, very old *Tert*$^{+/+}$ mice (92–125 wk of age) showed the same SMA positivity as 42–49-wk-old G3 *Tert*$^{-/-}$ mice (Fig. 2, A and C). In agreement with increased peribronchial fibroblast activation, we also found increased collagen deposits in the peribronchial areas (Masson's trichrome staining) and alveolar areas (Sirius Red) with increasing age in both *Tert*$^{+/+}$ and G3 *Tert*$^{-/-}$ mice, with G3 *Tert*$^{-/-}$ mice showing an anticipation of the phenotype with a similarly high percentage of alveolar and peribronchial collagen content in 42- to 49-wk-old G3 *Tert*$^{-/-}$ mice compared with very old (92–125-wk-old) wild-type mice (Fig. 2, A, D, and E).

Aging leads to increased DNA damage, apoptosis, and senescence in wild-type lungs, and this is anticipated in telomerase-deficient mice

Accumulation of cells with DNA damage is associated with aging, as well as with the presence of short telomeres in mice (López-Otín et al., 2013; Herrera et al., 1999b; Samper et al., 2001; Bernardes de Jesus et al., 2012). A marker for double-stranded DNA breaks and dysfunctional telomeres is phosphorylation of γ-H2AX (D'adda et al., 2003; Takai et al., 2003). Here, we set out to quantify γ-H2AX–positive cells in the lungs of *Tert*$^{+/+}$ and *G3 Tert*$^{-/-}$ mice at different ages. We observed increased γ-H2AX–positive cells per HPF with age in the alveolar parenchyma both in *Tert*$^{+/+}$ and G3 *Tert*$^{-/-}$ mice, with G3 *Tert*$^{-/-}$ mice showing an anticipation of the phenotype at all ages and with 42–49-wk-old G3 *Tert*$^{-/-}$ mice reaching levels similar to very old (92–125-wk-old) wild-type mice (Fig. 3, A and B). Next, we determined apoptosis in lung alveolar parenchyma as measured by presence of activated caspase-3 (C3)–positive cells. Again, we found an increased number of C3-positive cells with age in both *Tert*$^{+/+}$ and G3 *Tert*$^{-/-}$ mice, with G3 *Tert*$^{-/-}$ mice showing an anticipation of the phenotype at all ages and with 42- to 49-wk-old G3 *Tert*$^{-/-}$ mice reaching levels similar to very old (92–125-wk-old) wild-type mice (Fig. 3, A and C).

Finally, we also measured presence of alveolar p16-positive cells, which are associated with senescence. Notably, we found an increase in p16-positive cells with age in the lungs of *Tert*$^{+/+}$ and G3 *Tert*$^{-/-}$ mice (Fig. 3, A and D). Interestingly, both *Tert*$^{+/+}$ and G3 *Tert*$^{-/-}$ mice showed an increased number of senescent macrophages (F4/80-p16–positive cells) with aging, with 42–49-wk-old G3 *Tert*$^{-/-}$ mice showing the same percentage of macrophages positive for p16 as very old (92–125-wk-old) wild-type mice (Fig. 3, A and E). The percentages of alveolar senescent cells positive for the macrophage marker F4/80 were 85.72% (8–9-wk-old *Tert*$^{+/+}$ mice), 88.24% and 89.59% (42–49-wk-old *Tert*$^{+/+}$ and *Tert*$^{-/-}$ mice, respectively), and 73.18% (92–125-wk-old *Tert*$^{+/+}$ mice), suggesting that most of the alveolar senescent cells were macrophages.

Aging leads to decreased proliferation of ATII and club cells in wild-type lungs, and this is anticipated in the absence of telomerase

As we observed increased DNA damage and senescence with aging in total lung cells, we next addressed proliferation of different lung cell types with aging in both *Tert*$^{+/+}$ and G3 *Tert*$^{-/-}$ mice. To this end, we performed double immunostainings of whole-lung sections with the proliferation marker Ki67 and the cell-specific markers SFTPC (ATII cells), SCGB1A1 (club cells), and F4/80 (alveolar macrophages [AMs]). In addition, we also performed double immunostainings with the differentiation marker SOX2 and SCGB1A1 (club cells) to detected differentiation of club cells both in *Tert*$^{+/+}$ and G3 *Tert*$^{-/-}$ mice at different ages (Fig. 4 A). We found a gradual reduction in proliferating ATII cells and club cells with increasing age in *Tert*$^{+/+}$ mice, which at 92–125 wk of age reached similarly low levels as 42–49-wk-old G3 *Tert*$^{-/-}$ mice (Fig. 4, A, B, and D). We obtained similar findings in the case of F4/80-positive AMs (Fig. 4, A and C). Interestingly, we also found that differentiation of club cells (SOX2-positive club cells) progressively increased with age in both *Tert*$^{+/+}$ and G3 *Tert*$^{-/-}$ lungs, with G3 *Tert*$^{-/-}$ lungs showing significantly more differentiated Sox2-positive club cells at 8–9 wk old and 42–49 wk old compared with wild-type mice, which at very old age (92–125 wk old) had similarly high levels of Sox2-positive cells as 42–49-wk-old G3 *Tert*$^{-/-}$ mice (Fig. 4, A and E).

To confirm *Tert* deficiency in G3 *Tert*$^{-/-}$ lungs, we analyzed *Tert* mRNA expression levels in total lung extracts of young (5 wk) and older (61–72 wk) *Tert*$^{+/+}$ and G3 *Tert*$^{-/-}$ mice. As expected, *Tert* mRNA expression was negligible in young and old G3 *Tert*$^{-/-}$ mice compared with age-matched *Tert*$^{+/+}$ mice (Fig. 4 F). Additionally, since macrophages have been recognized to play a significant role in IPF pathogenesis (Zhang et al., 2018), we assessed mRNA expression of markers of M1 (*Tnf*, *Il1b*, and *Il6*) and M2 (*Il4*, *Il10*, and *Il13*) macrophages in total lung extracts from young and older *Tert*$^{+/+}$ and G3 *Tert*$^{-/-}$ mice (Fig. 4, G–L). In general, a significant increase in the expression of these markers was anticipated in G3 *Tert*$^{-/-}$ compared with *Tert*$^{+/+}$ mice (Fig. 4, G–L). These results were supported by analysis of TNF, interleukin (IL)-6, IL-4, and IL-10 protein levels in lung homogenates (Fig. 4, M–P). In general, protein levels of these cytokines were significantly increased in young and old G3 *Tert*$^{-/-}$ mice compared with *Tert*$^{+/+}$ mice. Remarkably only IL-10 protein levels increased with the age in both G3 *Tert*$^{-/-}$ and *Tert*$^{+/+}$ mice (Fig. 4, M–P).

Impaired pulmonary surfactant activity in aged wild-type lungs is anticipated in telomerase-deficient mice

We next set out to address the potential age-derived biophysical changes in lung surfactant activity in both *Tert*$^{+/+}$ and *G3 Tert*$^{-/-}$ mice. To do so, we tested the biophysical properties of pulmonary surfactant isolated from bronchoalveolar lavages in a captive bubble surfactometer (Autilio and Pérez-Gil, 2019).

The adsorption and postexpansion adsorption (Fig. 5 A) into air–liquid interfaces of surfactant were both significantly better in the youngest *Tert*$^{+/+}$ mice (4–7 wk old) compared with *G3 Tert*$^{-/-}$ mice of several ages. However, the difference in surface active properties disappeared with increasing age of *Tert*$^{+/+}$ mice, from 23 wk on. Interestingly, 71–72-wk-old *Tert*$^{+/+}$ mice showed a further impairment in surfactant properties during dynamic cycles when compared with younger *Tert*$^{+/+}$ mice (4–7 or 23–34 wk old; Fig. 5 B). Once subjected to breathing-like conditions, physiological aging affected the capability of surfactant to

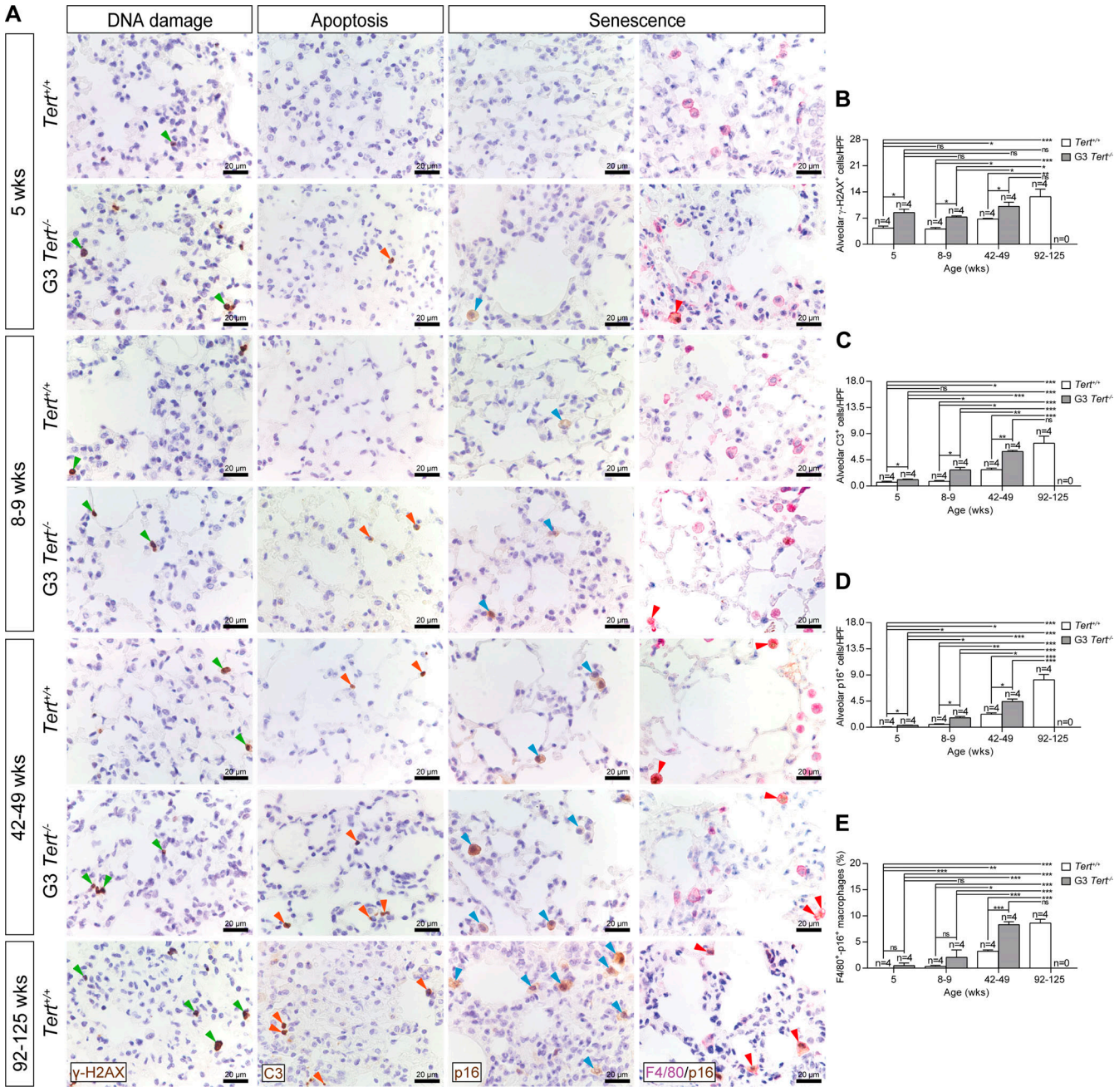

Figure 3. **Induced-telomere shortening and natural aging increase DNA damage, apoptosis, and macrophage senescence in the mouse lung. (A)** Representative immunostainings for alveolar γ-H2AX (brown, green arrowheads; left), activated C3 (brown, orange arrowheads; center left), p16 (brown, blue arrowheads; center right), and F4/80 and p16 (purple and brown, respectively; red arrowheads indicate double F4/80-p16-positive AMs; right) in *Tert*$^{+/+}$ and G3 *Tert*$^{-/-}$ mice at different time points. **(B–D)** Quantification of alveolar γ-H2AX–positive (B) and C3- positive (C), and p16-positive (D) cells, and double F4/80-p16-positive AMs (%; E). Quantifications were performed on five different alveolar areas in a random way. Data are expressed as mean ± SEM (n = 4 animals per group). *, P < 0.05; **, P < 0.01; ***, P < 0.001 (Shapiro–Wilk, Kruskal–Wallis, and Dunn–Sidak multiple comparison test). ns, not significant.

achieve γ values <9 mN/m under the conditions tested, leading to high relative area of compression (Fig. 5 B) and low stability of interfacial films (Fig. S1 A). This reduced surfactant activity was anticipated in G3 *Tert*$^{-/-}$ mice that already showed an early worsening in the relative area of compression at 4–7 wk of age (Fig. 5 B). Similarly, at 23 wk of age, G3 *Tert*$^{-/-}$ mice presented a significantly higher minimum γ when compared with *Tert*$^{+/+}$ mice of the same age (Fig. 5 B).

The content in surfactant proteins SP-B and SP-C also tended to decrease in G3 *Tert*$^{-/-}$ mice with increasing age (Fig. S1 B). As described for both healthy mice (Mahavadi et al., 2010) and neonates without lung disease (Autilio et al., 2020), the levels of SP-B and SP-C at the extracellular lavage exhibit a substantial variability in the control group. Moreover, the extreme hydrophobicity of SP-B and SP-C and their strong association with lipids typically make their Western blot (WB) bands appear

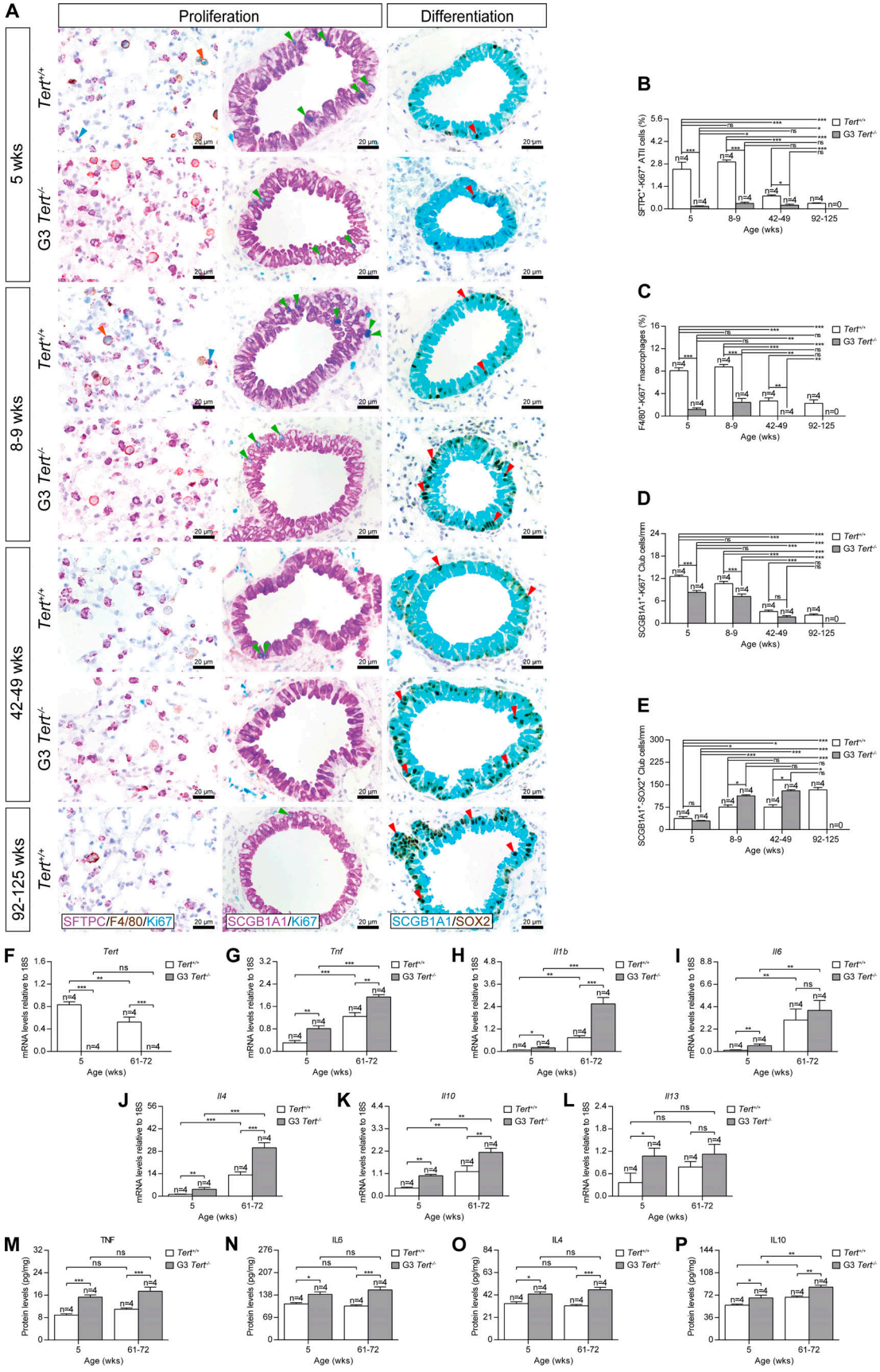

Figure 4. **Premature telomere shortening and natural aging reduce the proliferation of ATII cells, macrophages, and club cells and increase the differentiation of club cells. (A)** Representative immunostainings for SFTPC (purple), F4/80(brown), and Ki67 (blue; orange and blue arrowheads indicate

double SFTPC-Ki67– and F4/80-Ki67–positive cells, respectively; left); SCGB1A1 (purple) and Ki67 (blue and green arrowheads indicate double SCGB1A1-Ki67–positive club cells; center), and SCGB1A1 (blue) and SOX2 (brown; red arrowheads indicate double SCGB1A1-SOX2–positive club cells; right) in *Tert*$^{+/+}$ and G3 *Tert*$^{-/-}$ mice at different time points. **(B–E)** Quantification of SFTPC-Ki67–positive (B), F4/80-Ki67–positive (C), SCGB1A1-Ki67–positive (D), and SCGB1A1-SOX2–positive (E) cells. **(F–L)** Changes in total lung mRNA expression levels of *Tert* (F) and total lung mRNA expression of *Tnf* (G), *Il1b* (H), and *Il6* (I; pro-inflammatory markers) and *Il4* (J), *Il10* (K), and *Il13* (L; anti-inflammatory markers) normalized to 18S expression, and (M–P) protein levels of TNF (M), IL-6 (N), IL-4 (O), and IL-10 (P) assessed in lung homogenates from young (5 wk) and older (61–72 wk) *Tert*$^{+/+}$ and G3 *Tert*$^{-/-}$ mice. Quantifications were performed on five different alveolar areas or bronchi in a random way. Data are expressed as mean ± SEM (n = 4 animals per group). *, P < 0.05; **, P < 0.01; ***, P < 0.001 (Shapiro–Wilk, Kruskal–Wallis, and Dunn–Sidak multiple comparison test). ns, not significant.

blurred, especially in the case of SP-C. In spite of this limitation, we could detect a significantly lower amount of the two proteins in the lung fluid at 23–34 wk of age, becoming only a trend when 71–72-wk-old *Tert*$^{+/+}$ and G3 *Tert*$^{-/-}$ mice were compared. This confirms a worsening in surfactant biophysical properties during physiological aging regardless of *Tert* presence, since surfactant proteins are required to stabilize the respiratory surface and facilitate breathing mechanics.

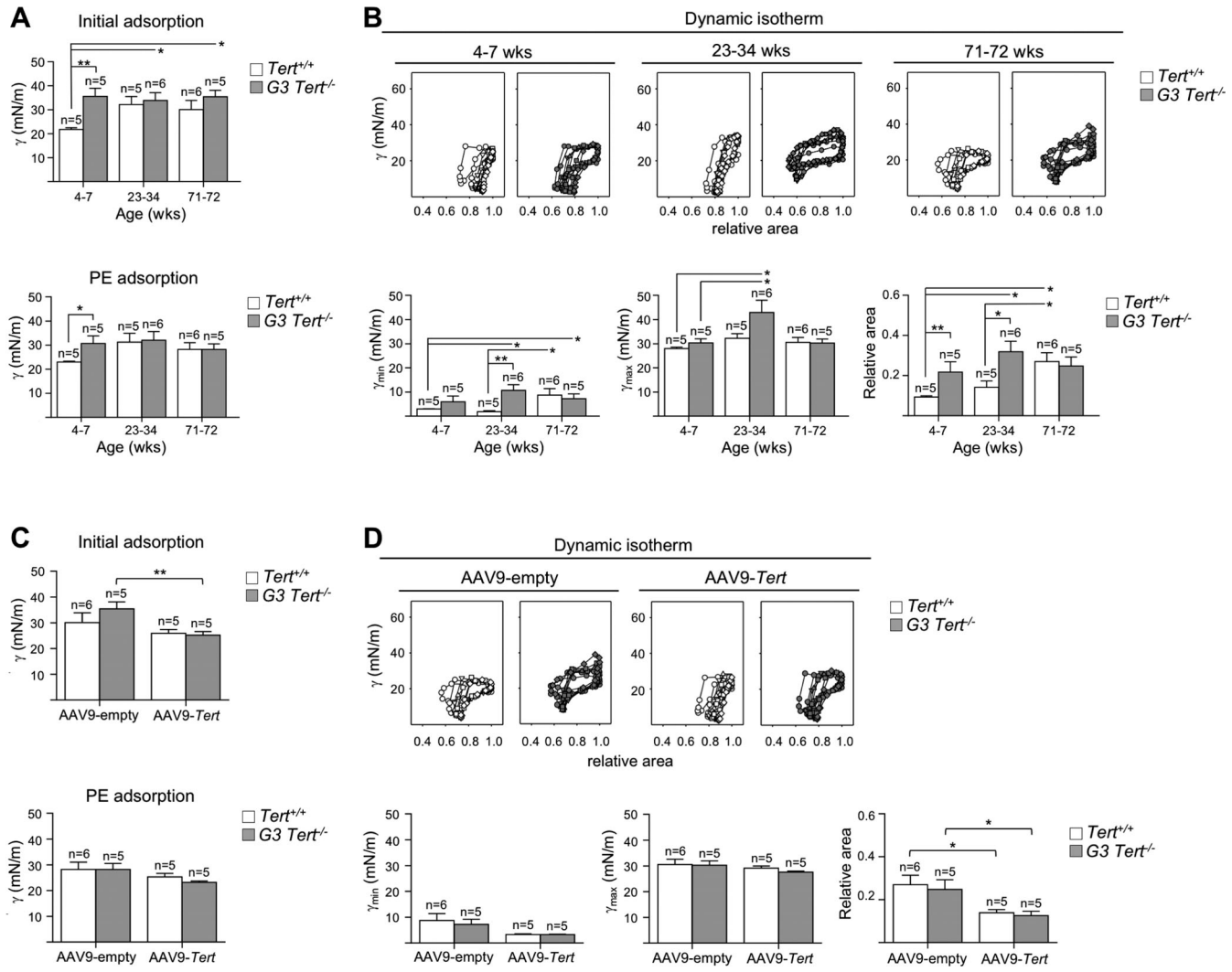

Figure 5. **Physiological aging leads to impaired surfactant activity which is partially restored by telomerase gene therapy in both wild-type mice and telomerase-deficient mice. (A and B)** Captive bubble results from *Tert*$^{+/+}$ and *G3* Tert$^{-/-}$ mice with increasing weeks of age. **(C and D)** Captive bubble results from 71–72-wk-old *Tert*$^{+/+}$ and *G3 Tert*$^{-/-}$ mice treated with AAV9-empty or AAV9-*Tert*. **(A and C)** Top: Surface tension obtained 1 s after applying surfactant onto the air bubble (initial adsorption). Bottom: Surface tension obtained 1 s after the bubble expansion (postexpansion [PE] adsorption). **(B and D)** Top: Representative γ-relative area isotherms obtained under breathing-like dynamic cycles for each group tested. Bottom: Minimum and maximum γ along with the relative area of compression obtained during the 20th cycle. White bars represent *Tert*$^{+/+}$ mice. Gray bars represent *G3 Tert*$^{-/-}$ mice. Data are expressed as mean ± SEM (n = 5–6 animals per group). *, P < 0.05; **, P < 0.01. Between different ages for each condition: One-way ANOVA with post hoc Dunn–Sidak multiple comparison test. Between different conditions within the same age: following a Shapiro–Wilk normality test, two-sample unpaired t test, or Mann–Whitney test when appropriate. γ, surface tension; max, maximum; min, minimum.

Telomerase gene therapy prevents lung fibrotic-like phenotypes in wild-type and telomerase-deficient mice

We previously showed that activation of telomerase in the lung using adeno-associated serotype 9 vector (AAV9)–Tert gene therapy vectors was sufficient to stop the progression of lung fibrosis in a mouse model of lung fibrosis owing to the presence of short telomeres and a sublethal dose of the lung-damaging agent bleomycin (Povedano et al., 2018). The fact that we show here that physiological aging leads to lung profibrotic phenotypes in wild-type mice that are anticipated in the context of telomerase-deficiency mice suggests that these phenotypes originate from telomere shortening with aging and that telomerase activation therapy should prevent or delay them.

Thus, here we set out to test whether telomerase gene therapy could delay or prevent lung profibrotic phenotypes associated with physiological aging in wild-type mice. As control, we also treated with telomerase gene therapy telomerase-deficient mice with short telomeres. To this end, 27–30-wk-old *Tert*$^{+/+}$ and G3 *Tert*$^{-/-}$ mice received an intravenous injection of either AAV9-*Tert* or AAV9-null virus particles, and these mice were followed until their end point (week 21; Fig. 6 A). First, we measured total lung mRNA expression of *Tert* by quantitative PCR (qPCR) to confirm *Tert* overexpression in these mice. We found that both *Tert*$^{+/+}$ and G3 *Tert*$^{-/-}$ mice treated with AAV9-*Tert* showed significantly increased *Tert* mRNA levels 21 wk after treatment compared with the corresponding mice treated with the AAV9-null vectors (Fig. 6 B). Next, we determined telomere length in the alveolar parenchyma and bronchi of these mice using immuno–telomere Q-FISH to evaluate the mean telomere fluorescence (mean telomere spot intensity) and the percentage of short telomeres in the indicated cell types. We found that both *Tert*$^{+/+}$ and G3 *Tert*$^{-/-}$ mice treated with AAV9-*Tert* showed increased mean telomere fluorescence and significantly decreased percentage of short telomeres in ATII and club cells compared with the corresponding mice treated with the AAV9-null vectors (Fig. 6, C–F and I).

Next, we set out to study whether AAV9-*Tert* treatment rescued the numbers of ATII cells and club cells in the lung by performing immunostainings with SFTPC and SCGB1A1, respectively. We found that both *Tert*$^{+/+}$ and G3 *Tert*$^{-/-}$ mice treated with AAV9-*Tert* showed significantly increased numbers of ATII and club cells (Fig. 6, G–I), indicating a recovery of lung cellularity. The increased number of ATII cells in wild-type mice upon treatment with AAV9-*Tert* was confirmed by increased transcriptional levels of different surfactant genes produced by ATII cells, including *Sftpa1*, *Sftpb*, and *Sftpd*, compared with AAV9-null–treated wild-type mice (Fig. 6, J–L). In the case of G3 *Tert*$^{-/-}$ mice treated with AAV9-*Tert*, we observed a tendency toward an increase in the expression of these genes, but this was not statistically significant (Fig. 6, J–L).

Telomerase gene therapy prevents fibrotic-like phenotypes in aged wild-type and telomerase-deficient mice

Next, we set out to address whether treatment with telomerase gene therapy also prevented fibrotic phenotypes with aging in both *Tert*$^{+/+}$ and G3 *Tert*$^{-/-}$ mice. We found that both *Tert*$^{+/+}$ and G3 *Tert*$^{-/-}$ mice treated with AAV9-*Tert* showed significantly decreased numbers of fibroblasts in the lung, as indicated by a decreased percentage of vimentin-positive area per HPF compared with the corresponding cohorts treated with the null vector (Fig. 7, A and B). We also detected a significant decrease in fibroblast activation by reduced percentage of peribronchial SMA-positive area in both *Tert*$^{+/+}$ and G3 *Tert*$^{-/-}$ mice treated with AAV9-*Tert* compared with the corresponding cohorts treated with the null vector (Fig. 7, A and C). Finally, we also observed a decreased percentage of alveolar collagen content per HPF (Sirius Red) and peribronchial collagen content deposits (Masson's trichrome staining) in both *Tert*$^{+/+}$ and G3 *Tert*$^{-/-}$ mice treated with AAV9-*Tert* compared with the corresponding cohorts treated with the null vector (Fig. 7, A, D, and E).

Telomerase gene therapy prevents DNA damage, senescence, and apoptosis in aged wild-type and telomerase-deficient mice lungs

Next, we determined the impact of AAV9-*Tert* gene therapy in rescuing DNA damage, apoptosis, and senescence in *Tert*$^{+/+}$ and G3 *Tert*$^{-/-}$ lungs treated with either AAV9-*Tert* or AAV9-null virus particles (Fig. 8). We found that both *Tert*$^{+/+}$ and G3 *Tert*$^{-/-}$ mice treated with AAV9-*Tert* showed significantly decreased numbers of γ-H2AX–positive cells per HPF in the lung parenchyma compared with the corresponding cohorts treated with the null vector (Fig. 8, A and B), indicating decreased DNA damage upon telomerase treatment. Similarly, we detected significantly decreased numbers of activated caspase3-positive cells in the alveolar parenchyma of both *Tert*$^{+/+}$ and G3 *Tert*$^{-/-}$ lungs treated with AAV9-*Tert* compared with those treated with the null vector (Fig. 8, A and C). Interestingly, increased senescence as detected by p16-positive cells specifically in the case of AMs was also rescued in both *Tert*$^{+/+}$ and G3 *Tert*$^{-/-}$ lungs treated with AAV9-*Tert* compared with those treated with the null vector (Fig. 8, A, D, and E).

Finally, by performing double immunostainings with the proliferation marker Ki67 and the specific markers SFTPC (ATII cells), SCGB1A1 (club cells), and F4/80 (AMs), we observed that proliferation of ATII cells, club cells, and AMs was significantly increased in both *Tert*$^{+/+}$ and G3 *Tert*$^{-/-}$ lungs treated with AAV9-*Tert* compared with those treated with the null vector (Fig. 9, A–D). Interestingly, the number of SOX2-positive differentiating club cells was also significantly reduced in *Tert*$^{+/+}$ and *Tert*$^{-/-}$ lungs upon telomerase gene therapy (Fig. 9, A and E).

Finally, to address whether treatment with telomerase gene therapy also prevented expression of proinflammatory and anti-inflammatory markers, we determined mRNA expression of *Tnf*, *Il1b*, *Il6*, *Il4*, *Il10*, and *Il13* in total lung extracts from *Tert*$^{+/+}$ and G3 *Tert*$^{-/-}$ mice (Fig. 9, F–K). We observed significantly decreased expression of these markers in both *Tert*$^{+/+}$ and G3 *Tert*$^{-/-}$ mice treated with AAV9-*Tert* compared with those treated with the null vector (Fig. 9, F–K). These findings were also supported by decreased protein levels of TNF, IL-6, IL-4, and IL-10 in lung homogenates from *Tert*$^{+/+}$ and G3 *Tert*$^{-/-}$ mice upon treatment with AAV9-*Tert* (Fig. 9, L–O).

Telomerase gene therapy prevents age-related impairment of surfactant activity in wild-type and telomerase-deficient mice

Finally, we addressed whether treatment with telomerase gene therapy improves age-related pulmonary surfactant inactivation

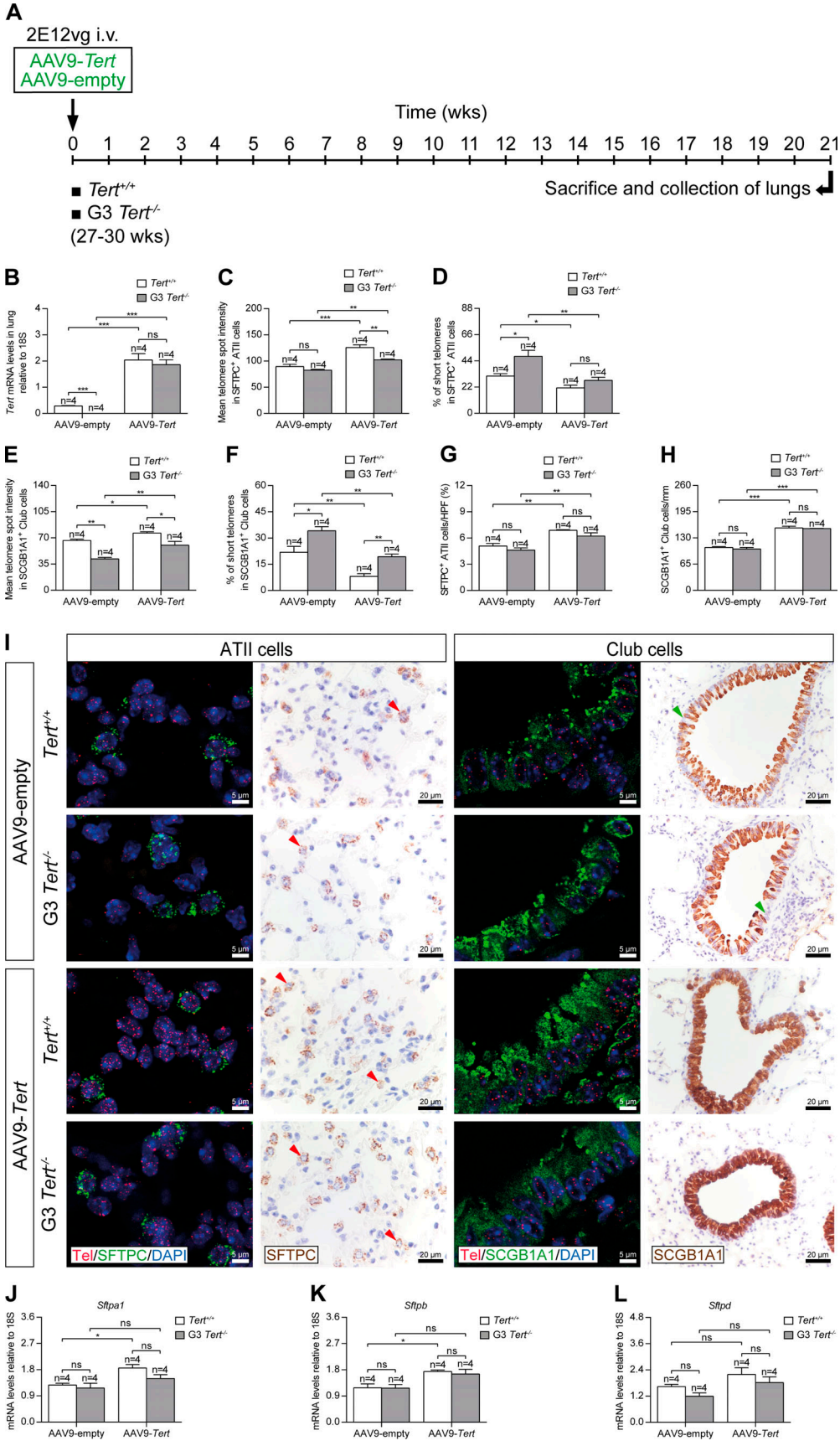

Figure 6. **Telomerase gene therapy in the mouse lung results in telomere elongation and increased number of ATII and club cells. (A)** Experimental protocol for the administration of AAV9-*Tert* and AAV9-empty virus. 27–30-wk-old *Tert*$^{+/+}$ and G3 *Tert*$^{-/-}$ mice were administered with 2E12vg of AAV9-*Tert*

and AAV9-empty virus by intravenous tail injection. Animals were sacrificed 21 wk later for lung tissue harvesting. **(B)** Total lung mRNA levels of *Tert* normalized to 18S expression in AAV9-empty– and AAV9-*Tert*–treated animals. **(C–H)** Quantification of mean telomere fluorescence (mean spot intensity; C and E), percentage of short telomeres in ATII and club cells corresponding to the 20th percentile of the fluorescence intensity values of controls (5-wk-old $Tert^{+/+}$ mice; D and F), and SFTPC-positive ATII cells (%) and SCGB1A1-positive club cells per epithelium length (millimeters) in AAV9-*Tert*– and AAV9-empty–treated mice (G and H). **(I)** Representative images showing a Q-FISH for telomere spot fluorescence in ATII and club cells (Cy3Tel probe [red], SFTPC- and SCGB1A1-positive cells [green], and nuclei stained with DAPI [blue]; left and center right), and SFTPC (brown, red arrowheads; center left) and SCGB1A1 (brown, green arrowheads; right) immunostainings in lung sections from $Tert^{+/+}$ and G3 $Tert^{-/-}$ mice treated with the AAV9-*Tert* (upper panels) or AAV9-empty (lower panels) virus. **(J–L)** Changes in total lung mRNA expression levels of the surfactant markers *Sftpa1*, *Sftpc*, and *Sftpd* normalized to 18S expression. Quantifications were performed on five different alveolar areas or bronchi in a random way. Data are expressed as mean ± SEM (n = 4 animals per group). *, P < 0.05; **, P < 0.01; ***, P < 0.001 (Shapiro–Wilk, Kruskal–Wallis, and Dunn–Sidak multiple comparison test). ns, not significant.

in both $Tert^{+/+}$ and G3 $Tert^{-/-}$ mice. To that end, we compared the activity of surfactant obtained from 71- to 72-wk-old G3 $Tert^{-/-}$ and $Tert^{+/+}$ mice treated with AAV9-empty or AAV9-*Tert*. We found that telomerase gene therapy significantly improved surfactant interfacial properties of old mice. G3 $Tert^{-/-}$ mice treated with AAV9-*Tert* showed an enhanced surfactant adsorption with reduced relative area of compression during dynamic cycles (Fig. 5, C and D) when compared with the animals treated with AAV9-empty. Similarly, surfactant from $Tert^{+/+}$ mice treated with telomerase exhibited a significant decrease in relative area of compression (Fig. 5 D) compared with AAV9-empty group.

Interestingly, telomerase gene therapy did not change SP-B and SP-C content in G3 $Tert^{-/-}$ mice but significantly reduced the amount of SP-B in $Tert^{+/+}$ mice (Fig. S2 B), with a tendency to decrease SP-C content. This may be due to a therapy-mediated rebalance of surfactant homeostasis that is more evident when endogenous *Tert* is also present.

Discussion

In spite of the recent introduction of two new antifibrotic drugs for the treatment of IPF, pirfenidone and nintedanib, there is still no cure for IPF, a devastating chronic progressive interstitial lung disease with a poor prognosis, with a median survival from the time of diagnosis of <4 yr (Richeldi et al., 2017; Martinez et al., 2017; Raghu et al., 2018; Somogyi et al., 2019). Thus,

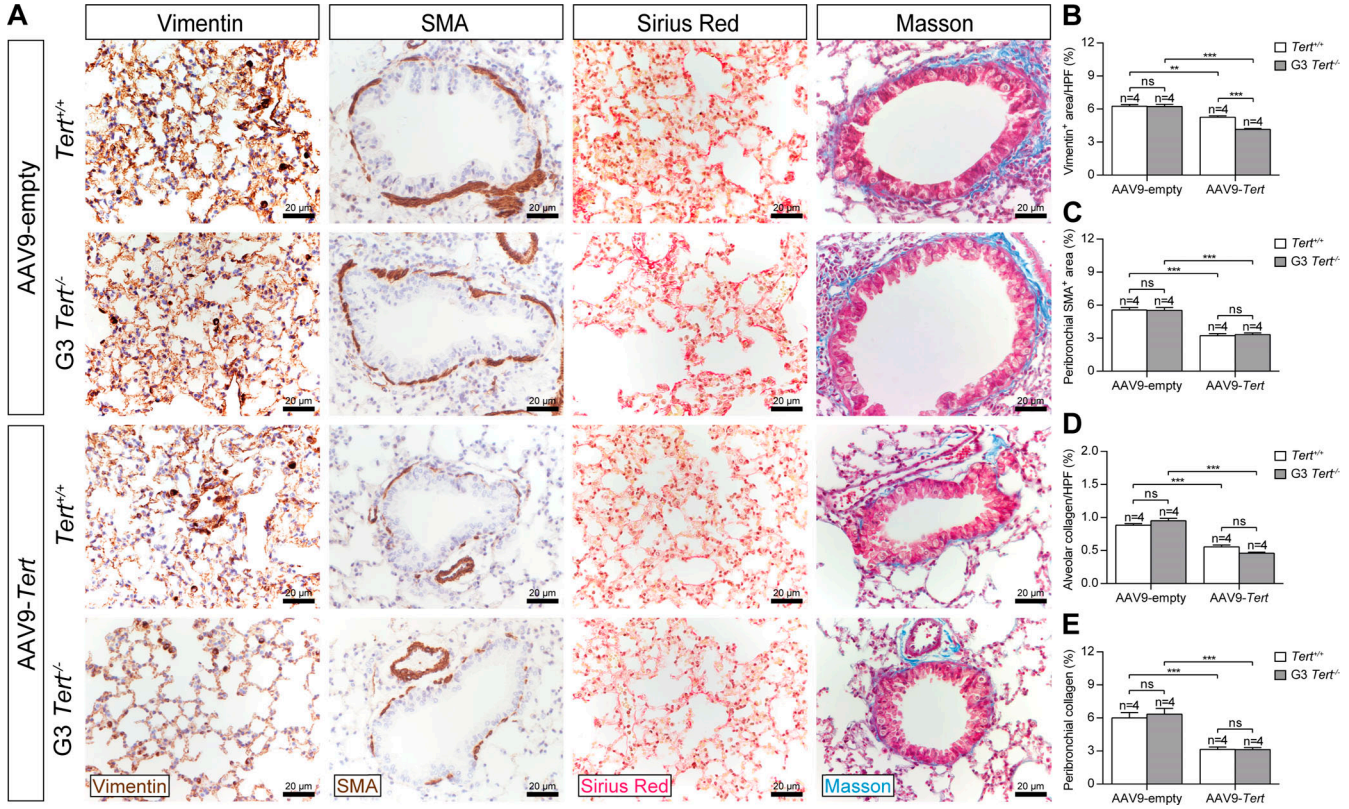

Figure 7. **AAV9-*Tert* treatment reduces fibroblast presence and activation and collagen deposition in the mouse lung. (A)** Representative images of vimentin (brown; left) and SMA (brown; center left) immunostainings and Sirius Red (red; center right) and Masson (blue; right) stainings in lung sections from $Tert^{+/+}$ and G3 $Tert^{-/-}$ mice treated with the AAV9-*Tert* (upper panels) or AAV9-empty (lower panels) virus. **(B–E)** Quantification of vimentin-positive (fibroblast marker) area per HPF (%; B), peribronchial SMA-positive (fibroblast activation marker) area (%; C), alveolar collagen content per HPF (%; D), and peribronchial collagen content (%; E). Quantifications were performed on five different alveolar areas or bronchi in a random way. Data are expressed as mean ± SEM (n = 4 animals per group). **, P < 0.01; ***, P < 0.001 (Shapiro–Wilk, Kruskal–Wallis and Dunn–Sidak multiple comparison test). ns, not significant.

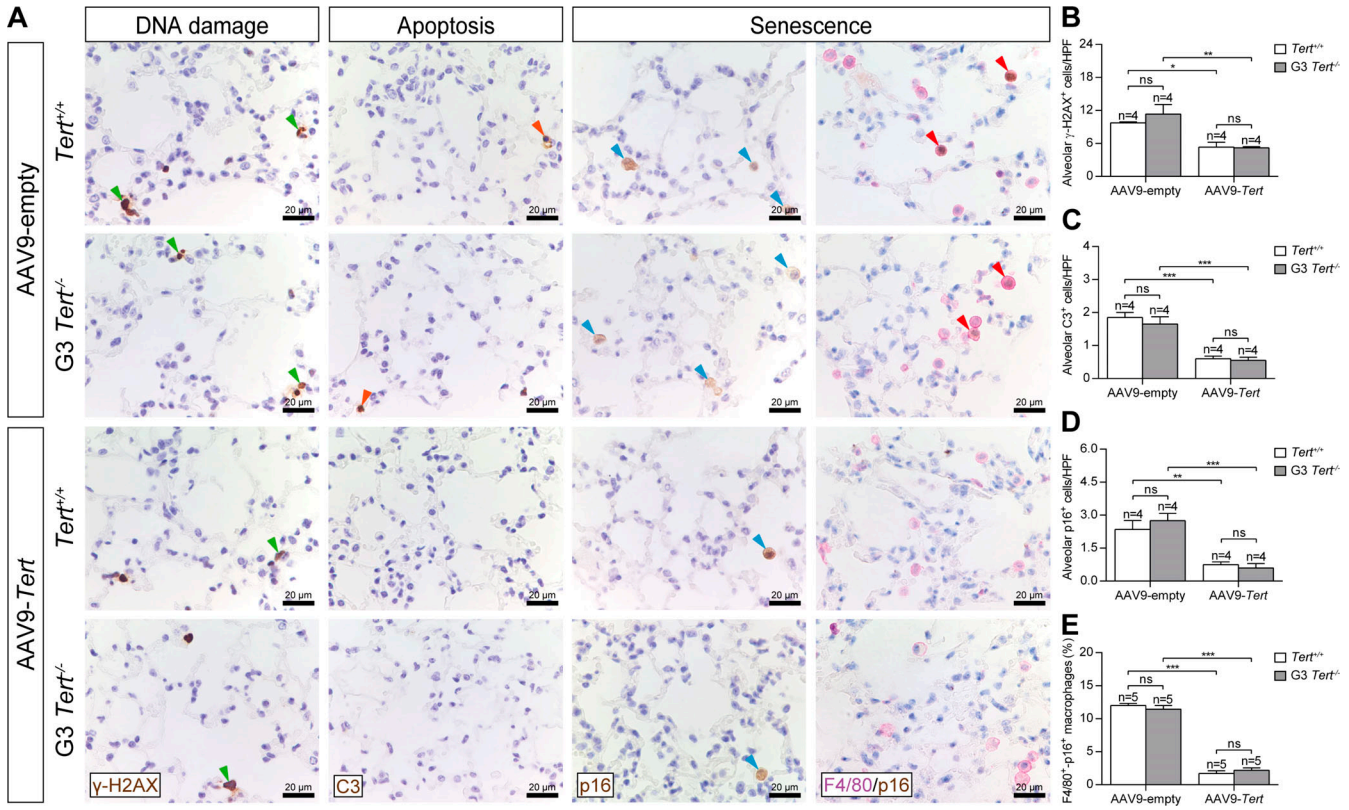

Figure 8. **Telomerase gene therapy ameliorates DNA damage, apoptosis, and macrophage senescence in the mouse lung. (A)** Representative immunostainings for alveolar γ-H2AX (brown, green arrowheads; left), activated C3 (brown, orange arrowheads; center left), p16 (brown, blue arrowheads; center right), and F4/80 and p16 (purple and brown, respectively; red arrowheads indicate double F4/80-p16–positive AMs; right) in lungs of *Tert*$^{+/+}$ and G3 *Tert*$^{-/-}$ mice treated with the AAV9-*Tert* (upper panels) or AAV9-empty (lower panels) virus. **(B–E)** Quantification of alveolar γ-H2AX–positive (B), C3-positive (C), and p16-positive (D) cells and double F4/80-p16–positive AMs (%; E). Quantifications were performed on five different alveolar areas in a random way. Data are expressed as mean ± SEM (n = 4–5 animals per group). *, P < 0.05; **, P < 0.01; ***, P < 0.001 (Shapiro–Wilk, Kruskal–Wallis and Dunn–Sidak multiple comparison test). ns, not significant.

additional hypotheses on the origin of IPF are necessary to drive new, more effective therapeutic approaches. Indeed, pirfenidone and nintedanib show anti-inflammatory and antifibrotic activity and slow IPF progression, but they are not curative (Ahluwalia et al., 2014; King et al., 2014; Hunninghake, 2014; Karimi-Shah and Chowdhury, 2015). We have recently demonstrated that AAV9-*Tert* therapy prevents the progression of pulmonary fibrosis in a mouse model of pulmonary fibrosis owing to presence of short telomeres (Povedano et al., 2018), thus demonstrating that short telomeres are at the origin of pulmonary fibrosis in mice and that elongation of short telomeres by telomerase can prevent progression of the disease. Remarkably, we did not find any deleterious effects of AAV9-*Tert* gene therapy in mice. In particular, we previously reported that AAV9-*Tert* gene therapy resulted in a significant increase in median and maximum life span accompanied by an amelioration of various age-associated phenotypes, including delayed cancer (Bernardes de Jesus et al., 2012). Moreover, we recently demonstrated AAV9-*Tert* therapy did not lead to an increase in cancer incidence or earlier onset of cancer in mice (Muñoz-Lorente et al., 2018).

In this regard, cellular aging is likely to be at the origin of IPF, as suggested by the fact that the incidence of IPF increases with age (Raghu et al., 2011; Faner et al., 2012; Selman and Pardo, 2014). Telomere shortening with age is considered one of the primary hallmarks of aging, and the presence of critically short telomeres owing to mutations in telomerase genes is associated with familial cases of IPF (Alder et al., 2008; Armanios et al., 2007; Tsakiri et al., 2007; Fingerlin et al., 2013; Cronkhite et al., 2008; Chibbar et al., 2010). A role for short/dysfunctional telomeres at the origin of IPF is also supported by genetically modified mouse models with mutations in telomerase or telomere maintenance genes (Povedano et al., 2015; Liu et al., 2018). In particular, we previously showed that a low bleomycin dose that does not induce pulmonary fibrosis in wild-type mice synergizes with short telomeres to trigger full-blown progressive pulmonary fibrosis in telomerase-deficient mice (Povedano et al., 2015). Similarly, induction of acute telomere dysfunction by abrogation of an essential telomere-protective protein, TRF1, specifically in ATII cells of the lung, is sufficient to induce progressive and lethal IPF in mice (Povedano et al., 2015). Thus, both in human patients and in mouse models, short/dysfunctional telomeres can induce IPF. Furthermore, ATII cells have been identified as a relevant cell type at the origin of the disease (Povedano et al., 2015).

To date, however, it remains uncertain whether physiological aging also leads to significant telomere shortening in the lungs

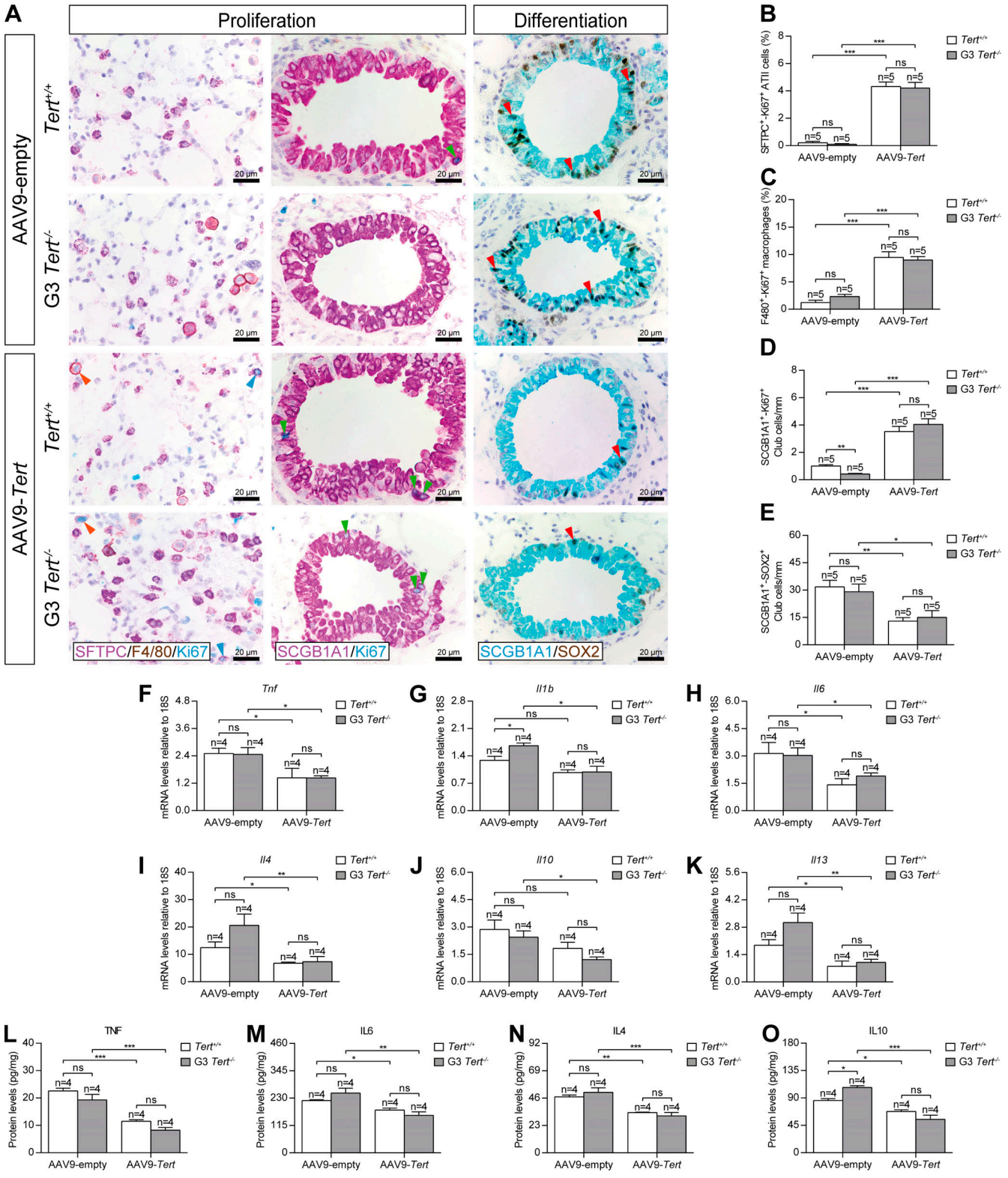

Figure 9. **Treatment with AAV9-*Tert* restores the proliferation of AT II cells, macrophages, and club cells and reduces the differentiation of club cells. (A)** Representative immunostainings for SFTPC (purple), F4/80 (brown), and Ki67 (blue; orange and blue arrowheads indicate double SFTPC-Ki67– and F4/80-Ki67–positive cells, respectively; left); SCGB1A1 (purple) and Ki67 (blue; green arrowheads indicate double SCGB1A1-Ki67–positive club cells; center); and SCGB1A1 (blue) and SOX2 (brown; red arrowheads indicate double SCGB1A1-SOX2–positive club cells; left) in lungs of *Tert*$^{+/+}$ and G3 *Tert*$^{-/-}$ mice treated with the AAV9-*Tert* (upper panels) or AAV9-empty (lower panels). **(B–E)** Quantification of SFTPC-Ki67–positive (B), F4/80-Ki67–positive (C), SCGB1A1-Ki67–positive (D), and SCGB1A1-SOX2–positive (E) cells. **(F–K)** Changes in total lung mRNA expression levels of *Tnf* (F), *Il1b* (G), and *Il6* (H; proinflammatory markers) and *Il4* (I), *Il10* (J), and *Il13* (K; anti-inflammatory markers) normalized to 18S expression and (L–O) protein levels of TNF (L), IL-6 (M), IL-4 (N), and IL-10 (O) assessed in lung homogenates from AAV9-empty– and AAV9-*Tert*–treated animals. Quantifications were performed on five different alveolar

areas or bronchi in a random way. Data are expressed as mean ± SEM (n = 4–5 animals per group). *, P < 0.05; **, P < 0.01; ***, P < 0.001 (Shapiro–Wilk, Kruskal–Wallis, and Dunn–Sidak multiple comparison test). ns, not significant.

and could be at the origin of a number of cases of sporadic IPF. In this regard, patients with sporadic IPF show shorter telomeres than normal healthy individuals (Tsang et al., 2012; Armanios and Blackburn, 2012; Armanios, 2013), and mice also show shorter telomeres in the lungs with increasing age (Birch et al., 2015). Here, we report that physiological aging in wild-type mice leads to telomere shortening in SCGB1A1-positive club cells and SFTPC-positive ATII cells, a phenomenon that is anticipated in telomerase-deficient mice (*Tert*$^{-/-}$ mice). In addition, we observe both reduced numbers and reduced proliferation of club cells and ATII cells with aging in wild-type mice, and again this phenotype is anticipated in telomerase-deficient mice. These findings suggest that telomere shortening associated with physiological aging can impair the stemness of bronchial club cells and ATII cells, which was previously shown to have epithelial stem/progenitor properties (Giangreco et al., 2002; Rawlins et al., 2009; Rock et al., 2011; Guha et al., 2012; Hogan et al., 2014; Kotton and Morrisey, 2014; Desai et al., 2014). Thus, these results presented here support the notion that telomere shortening with aging can impair the ability of stem cells to regenerate tissues (Blasco, 2007; Flores et al., 2008).

Further supporting this, we find here a significant increase of differentiating SOX2-positive club cells with aging, which again was anticipated in the telomerase-deficient mice. Sox2 has been previously shown a marker of differentiation of club cells (Tompkins et al., 2009), which is increased in bleomycin-induced pulmonary fibrosis in mice (Chuang et al., 2018), as well as in patients suffering from IPF (Plantier et al., 2011).

Interestingly, we also find here that mouse aging results in a reduced proliferation of the lung resident AMs and increased expression of M1 and M2 macrophage markers. Tissue-resident AMs are the most numerous immune cells present in the lung and have a key role in lung homeostasis by protecting the lung during tissue damage (Higashimoto et al., 1993; Boyd et al., 2012; Hussell and Bell, 2014; Byrne et al., 2015; Wong et al., 2017; Angelidis et al., 2019). Specifically, M1 macrophages contribute to tissue injury after excessive production of proinflammatory mediators (e.g., TNF, IL-1B, and IL-6), and M2 macrophages lead to resolution of inflammation and tissue repair upon anti-inflammatory cytokine activation (e.g., IL-4, IL-10, and IL-13; Zhang et al., 2018; Liu et al., 2019). M2 macrophages were reported to promote myofibroblast differentiation and are associated with pulmonary fibrogenesis (Hou et al., 2018). In this sense, overexpression of IL-6 and IL-10 were reported to impact the polarization of profibrotic M2 macrophages (Sun et al., 2011; Ayaub et al., 2017). In addition, IL-4 and IL-13 are required for the maintenance of pulmonary fibrosis (Jakubzick et al., 2003).

In line with shorter telomeres, wild-type mouse lungs show increased DNA damage, senescence, and apoptosis, together with an impairment in surfactant biophysical activity with increasing age, and this is anticipated in telomerase-deficient mice. Previous authors have also suggested a role for senescence in IPF (Selman and Pardo, 2014; Spagnolo et al., 2015; Pardo and Selman, 2017; Campisi, 2013). In particular, the effects observed on ATII and club cells in *Tert*$^{-/-}$ mice could be self-autonomous and/or a consequence of a different cellular environments. Indeed, senescent cells secrete inflammatory cytokines, chemokines, growth factors, and remodeling proteins that have autocrine and paracrine effects on the tissue microenvironment (Acosta et al., 2008; Kuilman et al., 2008; Parikh et al., 2019). As previously described by us, telomerase-deficient mice secret higher cytokine levels than wild-type mice (Mosteiro et al., 2016).

It is of particular interest that the majority of senescent cells were found to be AMs that have a crucial role in maintaining the correct surfactant homeostasis, preventing the accumulation of already used surfactant at the air–liquid interface with a limited biophysical performance (Autilio and Pérez-Gil, 2019). An impairment of surfactant activity has been already proposed as an early marker of fibrosis in a model of bleomycin-induced fibrosis in mice (Lopez-Rodriguez et al., 2016). It is therefore conceivable that the intrinsic deficiency in operative surfactant, both as a consequence of deactivated material that is not properly cleared by aged macrophages and the lack of enough amounts of newly synthetized surfactant by a reduced population of type II cells, leads to a progressively impaired pulmonary mechanics contributing ultimately to reduction in lung tissue elasticity and its abnormal remodeling.

Of relevance, we detected significantly increased collagen deposits with increasing age in wild-type lungs suggestive of early stages of IPF, which was anticipated in telomerase-deficient mice, again highlighting the role of short telomeres in the origin of these pathological findings. This is interesting, because previous studies have failed to detect lung fibrosis in the telomerase-deficient mouse model (Liu et al., 2007; Lee et al., 2009; Degryse et al., 2012).

Together, these molecular, cellular, biophysical, and pathological findings support that telomere shortening associated with wild-type mouse aging could be at the origin of fibrotic-like pathologies in mice. Here, we further demonstrate this hypothesis by rescuing these lung phenotypes at the molecular, cellular, biophysical, and pathological levels using an AAV9-based telomerase (*Tert*) gene therapy strategy, which has been previously shown by us to transduce lung cells, including ATII cells, and elongate telomeres (Povedano et al., 2018), as well as to block the progression of IPF in a mouse model of IPF which combined presence of short telomeres owing to telomerase deficiency and damage to the lungs using a low dose of bleomycin that did not induce IPF in wild-type mice (Povedano et al., 2015). In particular, treatment of old wild-type mice with AAV9-*Tert* rescued the proliferative defects of club cells, ATII cells, and resident AMs and rescued senescence, apoptosis, DNA damage, and pulmonary surfactant activity, as well as all signs of fibrosis, in aged wild-type mice.

In summary, here we demonstrate that telomerase gene therapy prevents the onset of lung degenerative and profibrotic

pathologies associated with physiological aging in wild-type and telomerase-deficient mice. These findings contribute to a better understanding of the importance of TERT as a potential target for future therapeutic approaches in IPF, especially in patients in whom pulmonary fibrosis is associated with short telomeres.

Materials and methods

Mice and ethical statement

Tert heterozygous mice were generated as previously described (Liu et al., 2000) and backcrossed to >98% C57/BL6 background. $Tert^{+/-}$ mice were intercrossed to generate $Tert^{+/+}$ and first-generation (G1) homozygous $Tert^{-/-}$ knockout mice. Second-generation (G2) $Tert^{-/-}$ mice were generated by successive breeding of G1 $Tert^{-/-}$ and then G3 $Tert^{-/-}$ mice by crosses between G2 $Tert^{-/-}$ mice (Fig. 1 A). Finally, $Tert^{+/+}$ and *G3* $Tert^{-/-}$ mice were used for aging experiments for which lungs of these mice where collected at different time points (Fig. 1 B). These mice were also used for telomerase gene therapy assays (Fig. 6 A). Experimental groups were composed by male (70%) and female (30%) mice in the case of molecular, cellular and pathological characterization. In addition, only male mice were used for the biophysical characterization. It should be noted that no significant differences were found between sexes in any of the experiments performed (data not shown). All animals were bred and maintained under specific pathogen–free conditions in laminar flow caging at the Spanish National Cancer Centre animal facility in accordance with the recommendations of the Federation of European Laboratory Animal Science Associations. All animal procedures were approved by the CNIO Institutional Animal Care and Use Committee and the Ethics Committee for Research and Animal Welfare.

Viral particle production and treatment

Viral vectors were generated by triple transfection of HEK293 cells and purified as previously described (Matsushita et al., 1998; Ayuso et al., 2010). Cells were cultured in roller bottles (Corning) in DMEM supplemented with 10% FBS to 80% confluence and cotransfected with a plasmid carrying the expression cassette flanked by the AAV2 viral inverted terminal repeats, a helper plasmid carrying the AAV rep2 and cap9 genes, and a plasmid carrying the adenovirus helper functions (plasmids kindly provided by K.A. High, Children's Hospital of Philadelphia, Philadelphia, PA). The expression cassettes were under the control of the cytomegalovirus promoter and contained a SV40 polyA signal for eGFP, and the cytomegalovirus promoter and the 3′-untranslated region of the *Tert* gene as polyA signal for *Tert*. AAV9 particles were purified using two cesium chloride gradients, dialyzed against PBS, filtered, and stored at −80°C until use. Then, 27–30-wk old $Tert^{+/+}$ and G3 $Tert^{-/-}$ mice were administered with 2E12vg of AAV9-*Tert* and AAV9-empty virus particles in a volume of 100 µl 0.001% Pluronic F-68 in PBS 1X by a single intravenous tail injection (Fig. 6 A). Pluronic F-68 was used to prevent aggregations of the virus particles (Foust et al., 2009). Animals were then sacrificed 21 wk after the administration of the AAV9-*Tert* and AAV9-empty virus particles.

Lung tissue collection and preparation

Before tissue collection, animals were euthanized by intraperitoneal injection of 10 µl/g of a ketamine/xylazine anesthetic combination in saline (100:10 mg/kg, respectively). Following dissection, lungs from $Tert^{+/+}$ and *G3* $Tert^{-/-}$ mice of the natural aging groups were harvested, fixed in 4% formaldehyde, and subsequently embedded in paraffin for histopathology and immunohistochemistry. In the case of $Tert^{+/+}$ and *G3* $Tert^{-/-}$ mice destined for the telomerase gene therapy experiments, only the lefts lungs were processed for histopathology and immunohistochemistry, and right lung lobes were separated and snap frozen in liquid nitrogen and stored at −80°C for qPCR.

Telomere Q-FISH analysis

After deparaffinization and rehydration, tissues underwent antigen retrieval in 10 mM sodium citrate buffer, and permeabilization was performed in PBS 0.5% Triton X-100 for 3 h. Next, tissues were washed three times for 5 min each in PBS 1X, fixed in 4% formaldehyde for 5 min, washed three times for 5 min each in PBS, and dehydrated in a 70–90%–100% ethanol series (5 min each). Following air drying the slides, 30 µl of the telomere probe mix (10 mM TrisCl, pH 7.2, 25 mM $MgCl_2$, 9 mM citric acid, 82 mM Na_2HPO_4, 50% deionized formamide [Sigma-Aldrich], 0.25% blocking reagent [Roche], and 0.5 µg/ml Telomeric PNA probe [Panagene]) was added, and slides were incubated for 3 min at 85°C and then 1 h at room temperature in a wet chamber in the dark. Slides were washed twice for 15 min each in 10 mM TrisCl (pH 7.2) and 0.1% BSA in 50% formamide and then three times for 5 min each in TBS 0.08% Tween 20. The tissues were then washed three times for 5 min each in PBS 0.1% Triton X-100, blocked with 10% donkey serum in PBS 0.1% Triton X-100 for 1 h, and incubated overnight at 4°C with rabbit prosurfactant protein C (AB3786, 1:200; EMD Millipore) and mouse CC10 (clone E-11, sc-365992, 1:200; Santa Cruz Biotechnology) antibodies. After three washes with PBS 0.1% Triton X-100, tissues were incubated with secondary antibodies for 1 h, washed three times for 5 min each in PBS 1X, and then mounted with Vectashield mounting media with DAPI (Vector Laboratories). Confocal images (40× magnification, 2× zoom, NA 1.25) were acquired as stacks using an SP5-WLL confocal microscope (Leica Microsystems), and maximum projection images were created with the LAS AF 2.7.3.9723 software. Telomere signal intensity was quantified using Definiens Developer Cell software version XD 64 2.5. For each analysis, three visual fields per section were scored.

Histopathological analyses and immunostaining

Paraffin-embedded lungs were cut into 3-µm sections for histopathological evaluation or immunohistochemistry. Sirius Red (Sigma-Aldrich) and Masson's trichrome (Dako) stainings were performed following manufacturer guidelines for the quantification of alveolar and peribronchial collagen content (%). Rabbit vimentin (clone D21H3, 5741, 1:50; Cell Signaling Technology) and mouse SMA (clone 1A4, IR611, 1:4; Dako and Agilent Technologies) antibodies were used for the determination of vimentin and peribronchial SMA-positive areas (%). Rabbit prosurfactant protein C (AB3786, 1:100; EMD Millipore) and goat

CC10 (clone T-18, sc-9772, 1:1,000; Santa Cruz Biotechnology) antibodies were used to determine the number of SFTPC-positive cells to total cell numbers (%) and the number of SCGB1A1-positive cells per epithelium length (millimeters). Rat F4/80 antibody (clone A3-1, MCA497, 1:20; AbD Serotec, and Bio-Rad) was used to determine the number of F4/80-positive macrophages. Mouse phospho-histone H2A.X (Ser139; clone JBW301, 05–636, 1:20; EMD Millipore), rabbit cleaved C3 (Asp175; 9661, 1:300; Cell Signaling Technology), and rat p16 (clone 33B; CNIO Monoclonal Antibodies Core Unit, Madrid, Spain) antibodies were used to assess the level of DNA damage (%) of SFTPC-positive ATII cells (SFTPC/H2AX) and the apoptosis and senescence rates (%) of SFTPC-positive ATII cells and F4/80-positive macrophages (SFTPC/F4/80/C3, SFTPC/p16, and F4/80/p16). Rabbit Ki-67 (clone D3B5, 12202, 1:50; Cell Signaling Technology) and rabbit SOX2 (clone C70B1, 3728, 1:75; Cell Signaling Technology) antibodies served to assess the level of proliferation (%) of SFTPC- and SCGB1A1-positive ATII and club cells and F4/80-positive macrophages (SFTPC/F4/80/Ki67 and SCGB1A1/Ki67) and the degree of differentiation of SCGB1A1-positive club cells (SCGB1A1/SOX2). All images (40× magnification, 2× optical zoom, NA 1.20) were acquired using the optical microscope Provis AX70 (Olympus) connected to a camera Olympus PM-C35DX. Olympus cellSens Entry 1.18 software was used to acquire images. Histological quantifications were performed on five different alveolar areas or five different bronchi in each case in a random way. The Fiji open-source image processing software package (http://fiji.sc) was used to quantify total cell numbers, epithelium length measurements, and the percentage of DAB (color deconvolution), Sirius Red, and Masson´s trichrome positive areas.

RNA isolation, reverse transcription, and qPCR

Inferior lung lobes from AAV9-*Tert* or AAV9-empty injected animals were homogenized in TRIzol (Invitrogen), and total RNA was treated with 2.72 KU/µl RNase-free DNase (Qiagen), purified using an RNeasy Mini Kit (Qiagen), and reverse transcribed to cDNA using SuperScript II First-Strand Synthesis System (Invitrogen) following the manufacturer specifications. The quantity and quality of total RNA was assessed on a NanoDrop Spectrophotometer (Thermo Fisher Scientific). cDNA samples were then amplified by qPCR in triplicate reactions for each primer pair assayed on a 7500 Real-Time PCR Instrument (Applied Biosystems) using SYBR Premix Ex Taq (Takara Bio) and the following qPCR conditions: 95°C for 2 min; 40 cycles of 95°C for 30 s, 60°C for 30 s and 95°C for 15 s, 60°C for 1 min, 95°C for 15 s, and 60°C for 15 s. Results were normalized using 18S rRNA gene (Rn18s) as endogenous control. The following primer pairs were used: *Tert*-F (Forward), 5′-TGACCAGCGTGTTAGGAAGA-3′; *Tert*-R (Reverse), 5′ CAGGAGGAAAGGA GCCAGAG-3′ (GenBank accession no. NM_009354.2); *Tnf*-F, 5′-GCCTCTTCTCATTCCTGCTTG-3′; *Tnf*-R, 5′-CTGATGAGAGGGAGGCCATT-3′ (GenBank accession no. NM_013693.3); *Il1b*-F, 5′-GCAACTGTTCCTGAACTCAACT-3′, *Il1b*-R 5′-ATCTTTTGGGGTCCGTCAACT3′ (GenBank accession no. NM_008361.3); *Il6*-F, 5′-ACGGCCTTCCCTACTTCACA-3′ and *Il6*-R, 5′-CATTTCCACGATTTCCCAGA-3′ (GenBank accession no. NM_031168.1); *Il4*-F, 5′-CCTCACAGCAACGAAGAACA-3′ and *Il4*-R, 5′-CGAAAAGCCCGAAAGAGTC-3′ (GenBank accession no. NM_021283.2); *Il10*-F, 5′-GCACTACCAAAGCCACAAGG-3′ and *Il10*-R, 5′-TAAGAGCAGGCAGCATAGCA-3′ (GenBank accession no. NM_ 010548.2); *Il13*-F, 5′-GCCTCCCCGATACCAAAAT-3′ and *Il13*-R, 5′-CTTCCTCCTCAACCCTCCTC-3′ (GenBank accession no. NM_008355.3); *Sftpa1*-F, 5′-CCATCGCAAGCATTACAAAG-3′ and *Sftpa1*-R, 5′-CACAGAAGCCCCATCCAG-3′ (GenBank accession no. NM_023134.4); *Sftpb*-F, 5′-CTGCTGCTTCCTACCCTCTG-3′ and *Sftpb*-R, 5′-ATCCTCACACTCTTGGCACA-3′ (GenBank accession no. NM_147779.2); *Sftpd*-F, 5′-TGAGAATGCTGCCATACAGC-3′ and *Sftpd*-R, 5′-GAATAGACCAGGGGCTCTCC-3′ (GenBank accession no. NM_009160.2); *Rn18s*-F, 5′-ATGCTCTTAGCTGAGTGTCCCG-3′ and *Rn18s*-R, 5′-ATTCCTAGCTGCGGTATCCAGG-3′ (GenBank accession no. NR_003278.3).

Pulmonary surfactant isolation and activity

Surfactant was collected from bronchoalveolar lavages of mice lungs as described before (Autilio et al., 2018). In detail, bronchoalveolar lavage supernatant was ultracentrifuged (100,000 *g*, 4°C, 1 h) and diluted with 5 mM Tris buffer containing 150 mM NaCl (5 mM; pH 7; Sigma-Aldrich) to reach a concentration of 10 mg/ml of phosphatidylcholine (PC). PC was tested in triplicate using an enzymatic colorimetric method (Spinreact; St. Esteve de Bas).

The interfacial activity of surfactant was measured in a captive bubble surfactometer as described before (Schürch et al., 2010) upon injection of 300 nl surfactant onto the surface of the air bubble. Initial adsorption was measured by monitoring the decay in surface tension (γ) during the first 5 min after surfactant injection and postexpansion adsorption during the 5 min after expansion of the bubble volume from 0.05 to 0.15 ml. Then, the bubble was subjected to rapid (30 cycles/min) physiological-like compression–expansion dynamics, changing its volume by ∼25%, and the corresponding isotherms were built upon representation of γ versus relative area of the bubble. Surfactant performance during cycling was evaluated by comparing minimum and maximum γ and the reduction in area required to reach the minimum γ. Finally, the mechanical stability of the surfactant films was assessed by registering the decay in γ occurring in compressed interfacial films as a consequence of the discharge of five shocking mechanical perturbations as previously described (Schürch et al., 2010).

WB analysis

WB was performed under reducing conditions as previous described (Lopez-Rodriguez et al., 2016). Since surfactant proteins are the only proteins present in the complex, we normalize our data, as previously reported (Autilio et al., 2020), by loading onto the gel equivalent amounts of PC per sample (3 µg from isolated mice surfactant). Therefore, changes in protein composition have to be interpreted as connected with changes in the quality of surfactant, seen as protein-to-lipid ratios.

Electrophoresis Laemmli buffer (2% SDS, 62.5 mM Tris, pH 6.8, 10% glycerol, and 0.03% bromophenol blue) containing 4% β-mercapto-ethanol was added to insolated mice surfactant before incubating (15 min; 90°C) and loading the samples. The

polyacrylamide gel (16%) was run for ∼1 h, and proteins were transferred onto polyvinylidene fluoride membranes with a semi-dry system (1 h; 4°C) and blocked in PBS-T (100 mM Na_2HPO_4/KH_2PO_4-1% Tween) with 5% skim milk at room temperature for 2 h. Membranes were then incubated overnight with the primary human/mouse polyclonal antibodies (1:5,000, anti-mature SP-B [WRAB-48604], 1:10,000 anti-mature SP-C [WRAB-76694; Seven Hills]) in PBS-T 5% milk at 4°C, washed thoroughly in PBS-T, and incubated with the secondary antibody (1:5,000, anti-rabbit [P0217]; Dako and Agilent) for 2 h at room temperature (E3). Membranes were then developed (1 min of exposition) using a commercial ECL system (Millipore). Bands densitometry was performed by using ImageJ for Mac OS X.

ELISAs

Superior right lung lobes were homogenized in RIPA Buffer (Thermo Fisher Scientific) containing a protease-phosphatase inhibitor mixture (Roche), and total protein concentration was determined with the Pierce BCA Protein Assay Kit (Thermo Fisher Scientific). Cytokine levels were assessed in homogenized lung tissue lysates using mouse IL-4, IL-10, IL-13, and TNF Quantikine ELISA Kits (R&D Systems), following the manufacturer's specifications, normalized to total lung protein levels.

Statistics

Statistical analyses were accomplished using SPSS Statistics Software v21 for Windows (IBM). Following a Shapiro–Wilk normality test, either a one-way ANOVA test or a Kruskal–Wallis test were used, and then the post hoc Dunn–Sidak multiple test was performed for multiple comparisons. According to the sample distribution, either a Mann–Whitney or unpaired *t* test was used to compare $Tert^{+/+}$ and G3 $Tert^{-/-}$ mice of the same age or 71–72-wk-old mice with and without telomerase therapy. Results are shown as mean values ± SEM. For all analyses, a P value < 0.05 was considered statistically significant.

Online supplemental material

Fig. S1 shows that the interfacial stability of surfactant material from $Tert^{+/+}$ mice under compression of the air–liquid interface is significantly reduced after 71–72 wk of physiological aging. Fig. S2 shows that telomerase therapy does not affect membrane stability but apparently reduces the content of SP-B in $Tert^{+/+}$ 71–72-wk-old mice.

Acknowledgments

Research in the Blasco Lab is funded by the Fundación Botín and Fundación Banco Santander (Spain); Instituto de Salud Carlos III, Spanish Ministry of Science and Innovation (DTS17/ 00152), cofunded European Regional Development Fund (ERDF); Spanish Estate Research Agency, Spanish Ministry of Science and Innovation (project RETOS SAF2017-82623-R), cofunded by ERDF and RyPSE-CM Programme (B2017/BMD-3770), Community of Madrid, cofunded by the European Social Fund and ERDF. The CNIO, certified as Severo Ochoa Excellence Centre, is supported by the Spanish Government through the Instituto de Salud Carlos III. C. Autilio and J. Pérez-Gil acknowledge funding from the Spanish Ministry of Science and Innovation (RTI2018-094564-B-100) and the Regional Government of Madrid (P2018/NMT-4389).

The authors declare no competing financial interests.

Author contributions: M.A. Blasco had the original idea and secured funding. M.A. Blasco, P. Martínez, F. Bosch, and J. Pérez-Gil supervised research. M.A. Blasco, P. Martínez, S. Piñeiro-Hermida, J. Pérez-Gil, and C. Autilio wrote the paper. S. Piñeiro-Hermida and C. Autilio analyzed the data and performed experiments.

Submitted: 21 February 2020
Revised: 23 June 2020
Accepted: 17 July 2020

References

Acosta, J.C., A. O'Loghlen, A. Banito, M.V. Guijarro, A. Augert, S. Raguz, M. Fumagalli, M. Da Costa, C. Brown, N. Popov, et al. 2008. Chemokine signaling via the CXCR2 receptor reinforces senescence. *Cell*. 133: 1006–1018. https://doi.org/10.1016/j.cell.2008.03.038

Ahluwalia, N., B.S. Shea, and A.M. Tager. 2014. New therapeutic targets in idiopathic pulmonary fibrosis. Aiming to rein in runaway wound-healing responses. *Am. J. Respir. Crit. Care Med*. 190:867–878. https://doi.org/10.1164/rccm.201403-0509PP

Alder, J.K., J.J.L. Chen, L. Lancaster, S. Danoff, S.C. Su, J.D. Cogan, I. Vulto, M. Xie, X. Qi, R.M. Tuder, et al. 2008. Short telomeres are a risk factor for idiopathic pulmonary fibrosis. *Proc. Natl. Acad. Sci. USA*. 105: 13051–13056. https://doi.org/10.1073/pnas.0804280105

Angelidis, I., L.M. Simon, I.E. Fernandez, M. Strunz, C.H. Mayr, F.R. Greiffo, G. Tsitsiridis, M. Ansari, E. Graf, T.M. Strom, et al. 2019. An atlas of the aging lung mapped by single cell transcriptomics and deep tissue proteomics. *Nat. Commun*. 10:963. https://doi.org/10.1038/s41467-019-08831-9

Armanios, M.. 2013. Telomeres and age-related disease : how telomere biology informs clinical paradigms. *J. Clin. Invest*. 123:996–1002. https://doi.org/10.1172/JCI66370

Armanios, M., and E.H. Blackburn. 2012. The telomere syndromes. *Nat. Rev. Genet*. 13:693–704. https://doi.org/10.1038/nrg3246

Armanios, M.Y., J.J.L. Chen, J.D. Cogan, J.K. Alder, R.G. Ingersoll, C. Markin, W.E. Lawson, M. Xie, I. Vulto, J.A. Phillips, III, et al. 2007. Telomerase mutations in families with idiopathic pulmonary fibrosis. *N. Engl. J. Med*. 356:1317–1326. https://doi.org/10.1056/NEJMoa066157

Autilio, C., and J. Pérez-Gil. 2019. Understanding the principle biophysics concepts of pulmonary surfactant in health and disease. *Arch. Dis. Child. Fetal Neonatal Ed*. 104:F443–F451. https://doi.org/10.1136/archdischild-2018-315413

Autilio, C., M. Echaide, D. De Luca, and J. Pérez-Gil. 2018. Controlled hypothermia may improve surfactant function in asphyxiated neonates with or without meconium aspiration syndrome. *PLoS One*. 13. e0192295. https://doi.org/10.1371/journal.pone.0192295

Autilio, C., M. Echaide, S. Shankar-Aguilera, R. Bragado, D. Amidani, F. Salomone, J. Pérez-Gil, and D. De Luca. 2020. Surfactant Injury in the Early Phase of Severe Meconium Aspiration Syndrome. *Am. J. Respir. Cell Mol. Biol*. rcmb.2019-0413OC. https://doi.org/10.1165/rcmb.2019-0413OC

Ayaub, E.A., A. Dubey, J. Imani, F. Botelho, M.R.J. Kolb, C.D. Richards, and K. Ask. 2017. Overexpression of OSM and IL-6 impacts the polarization of pro-fibrotic macrophages and the development of bleomycin-induced lung fibrosis. *Sci. Rep*. 7:13281. https://doi.org/10.1038/s41598-017-13511-z

Ayuso, E., F. Mingozzi, J. Montane, X. Leon, X.M. Anguela, V. Haurigot, S.A. Edmonson, L. Africa, S. Zhou, K.A. High, et al. 2010. High AAV vector purity results in serotype- and tissue-independent enhancement of transduction efficiency. *Gene Ther*. 17:503–510. https://doi.org/10.1038/gt.2009.157

Bernardes de Jesus, B., E. Vera, K. Schneeberger, A.M. Tejera, E. Ayuso, F. Bosch, and M.A. Blasco. 2012. Telomerase gene therapy in adult and old mice delays aging and increases longevity without increasing cancer. *EMBO Mol. Med*. 4:691–704. https://doi.org/10.1002/emmm.201200245

Birch, J., R.K. Anderson, C. Correia-Melo, D. Jurk, G. Hewitt, F.M. Marques, N.J. Green, E. Moisey, M.A. Birrell, M.G. Belvisi, et al. 2015. DNA damage response at telomeres contributes to lung aging and chronic obstructive pulmonary disease. *Am. J. Physiol. Lung Cell. Mol. Physiol.* 309:L1124–L1137. https://doi.org/10.1152/ajplung.00293.2015

Blackburn, E.H.. 2001. Switching and signaling at the telomere. *Cell*. 106: 661–673. https://doi.org/10.1016/S0092-8674(01)00492-5

Blackburn, E.H., C.W. Greider, and J.W. Szostak. 2006. Telomeres and telomerase: the path from maize, Tetrahymena and yeast to human cancer and aging. *Nat. Med*. 12:1133–1138. https://doi.org/10.1038/nm1006-1133

Blasco, M.A.. 2005. Mice with bad ends: mouse models for the study of telomeres and telomerase in cancer and aging. *EMBO J*. 24:1095–1103. https://doi.org/10.1038/sj.emboj.7600598

Blasco, M.A.. 2007. Telomere length, stem cells and aging. *Nat. Chem. Biol*. 3: 640–649. https://doi.org/10.1038/nchembio.2007.38

Blasco, M.A., H.W. Lee, M.P. Hande, E. Samper, P.M. Lansdorp, R.A. DePinho, and C.W. Greider. 1997. Telomere shortening and tumor formation by mouse cells lacking telomerase RNA. *Cell*. 91:25–34. https://doi.org/10.1016/S0092-8674(01)80006-4

Boyd, A.R., P. Shivshankar, S. Jiang, M.T. Berton, and C.J. Orihuela. 2012. Age-related defects in TLR2 signaling diminish the cytokine response by alveolar macrophages during murine pneumococcal pneumonia. *Exp. Gerontol*. 47:507–518. https://doi.org/10.1016/j.exger.2012.04.004

Brandenberger, C., and C. Mühlfeld. 2017. Mechanisms of lung aging. *Cell Tissue Res*. 367:469–480. https://doi.org/10.1007/s00441-016-2511-x

Bueno, M., Y.C. Lai, Y. Romero, J. Brands, C.M. St Croix, C. Kamga, C. Corey, J.D. Herazo-Maya, J. Sembrat, J.S. Lee, et al. 2015. PINK1 deficiency impairs mitochondrial homeostasis and promotes lung fibrosis. *J. Clin. Invest*. 125:521–538. https://doi.org/10.1172/JCI74942

Byrne, A.J., S.A. Mathie, L.G. Gregory, and C.M. Lloyd. 2015. Pulmonary macrophages: key players in the innate defence of the airways. *Thorax*. 70:1189–1196. https://doi.org/10.1136/thoraxjnl-2015-207020

Campisi, J.. 2013. Aging, cellular senescence, and cancer. *Annu. Rev. Physiol*. 75:685–705. https://doi.org/10.1146/annurev-physiol-030212-183653

Canela, A., P. Klatt, and M.A. Blasco. 2007. Telomere length analysis. *In* Biological Aging. Methods in Molecular Biology. Vol. 371. T.O. Tollefsbol, editor. Humana Press, Totowa, NJ. 45–72., https://doi.org/10.1007/978-1-59745-361-5_5

Chibbar, R., J.A. Gjevre, F. Shih, H. Neufeld, E.G. Lemire, D.A. Fladeland, and D.W. Cockcroft. 2010. Familial interstitial pulmonary fibrosis: a large family with atypical clinical features. *Can. Respir. J*. 17:269–274. https://doi.org/10.1155/2010/591523

Chuang, H.M., L.I. Ho, M.H. Huang, K.L. Huang, T.W. Chiou, S.Z. Lin, H.L. Su, and H.J. Harn. 2018. Non-canonical regulation of type i collagen through promoter binding of sox2 and its contribution to ameliorating pulmonary fibrosis by butylidenephthalide. *Int. J. Mol. Sci*. 19. E3024. https://doi.org/10.3390/ijms19103024

Codd, V., C.P. Nelson, E. Albrecht, M. Mangino, J. Deelen, J.L. Buxton, J.J. Hottenga, K. Fischer, T. Esko, I. Surakka, et al; CARDIoGRAM consortium. 2013. Identification of seven loci affecting mean telomere length and their association with disease. *Nat. Genet*. 45:422–427–e2. https://doi.org/10.1038/ng.2528

Cronkhite, J.T., C. Xing, G. Raghu, K.M. Chin, F. Torres, R.L. Rosenblatt, and C.K. Garcia. 2008. Telomere shortening in familial and sporadic pulmonary fibrosis. *Am. J. Respir. Crit. Care Med*. 178:729–737. https://doi.org/10.1164/rccm.200804-550OC

D'adda, F., D. Fagagna, P.M. Reaper, L. Clay-Farrace, H. Fiegler, P. Carr, T. Von Zglinicki, G. Saretzki, N.P. Carter, and S.P. Jackson. 2003. A DNA damage checkpoint response in telomere-initiated senescence. *Nature*. 426:194–198. https://doi.org/10.1038/nature02118

de Lange, T.. 2005. Shelterin: the protein complex that shapes and safeguards human telomeres. *Genes Dev*. 19:2100–2110. https://doi.org/10.1101/gad.1346005

Degryse, A.L., X.C. Xu, J.L. Newman, D.B. Mitchell, H. Tanjore, V.V. Polosukhin, B.R. Jones, F.B. McMahon, L.A. Gleaves, J.A. Phillips, III, et al. 2012. Telomerase deficiency does not alter bleomycin-induced fibrosis in mice. *Exp. Lung Res*. 38:124–134. https://doi.org/10.3109/01902148.2012.658148

Demopoulos, K., D.A. Arvanitis, D.A. Vassilakis, N.M. Siafakas, and D.A. Spandidos. 2002. MYCL1, FHIT, SPARC, p16(INK4) and TP53 genes associated to lung cancer in idiopathic pulmonary fibrosis. *J. Cell. Mol. Med*. 6:215–222. https://doi.org/10.1111/j.1582-4934.2002.tb00188.x

Desai, T.J., D.G. Brownfield, and M.A. Krasnow. 2014. Alveolar progenitor and stem cells in lung development, renewal and cancer. *Nature*. 507: 190–194. https://doi.org/10.1038/nature12930

Faner, R., M. Rojas, W. Macnee, and A. Agustí. 2012. Abnormal lung aging in chronic obstructive pulmonary disease and idiopathic pulmonary fibrosis. *Am. J. Respir. Crit. Care Med*. 186:306–313. https://doi.org/10.1164/rccm.201202-0282PP

Fingerlin, T.E., E. Murphy, W. Zhang, A.L. Peljto, K.K. Brown, M.P. Steele, J.E. Loyd, G.P. Cosgrove, D. Lynch, S. Groshong, et al. 2013. Genome-wide association study identifies multiple susceptibility loci for pulmonary fibrosis. *Nat. Genet*. 45:613–620. https://doi.org/10.1038/ng.2609

Flores, I., M.L. Cayuela, and M.A. Blasco. 2005. Effects of telomerase and telomere length on epidermal stem cell behavior. *Science*. 309: 1253–1256. https://doi.org/10.1126/science.1115025

Flores, I., A. Canela, E. Vera, A. Tejera, G. Cotsarelis, and M.A. Blasco. 2008. The longest telomeres: a general signature of adult stem cell compartments. *Genes Dev*. 22:654–667. https://doi.org/10.1101/gad.451008

Foust, K.D., E. Nurre, C.L. Montgomery, A. Hernandez, C.M. Chan, and B.K. Kaspar. 2009. Intravascular AAV9 preferentially targets neonatal neurons and adult astrocytes. *Nat. Biotechnol*. 27:59–65. https://doi.org/10.1038/nbt.1515

Giangreco, A., S.D. Reynolds, and B.R. Stripp. 2002. Terminal bronchioles harbor a unique airway stem cell population that localizes to the bronchoalveolar duct junction. *Am. J. Pathol*. 161:173–182. https://doi.org/10.1016/S0002-9440(10)64169-7

Greider, C.W., and E.H. Blackburn. 1985. Identification of a specific telomere terminal transferase activity in Tetrahymena extracts. *Cell*. 43:405–413. https://doi.org/10.1016/0092-8674(85)90170-9

Guha, A., M. Vasconcelos, Y. Cai, M. Yoneda, A. Hinds, J. Qian, G. Li, L. Dickel, J.E. Johnson, S. Kimura, et al. 2012. Neuroepithelial body microenvironment is a niche for a distinct subset of Clara-like precursors in the developing airways. *Proc. Natl. Acad. Sci. USA*. 109:12592–12597. https://doi.org/10.1073/pnas.1204710109

Herrera, E., E. Samper, and M.A. Blasco. 1999a. Telomere shortening in mTR−/− embryos is associated with failure to close the neural tube. *EMBO J*. 18:1172–1181. https://doi.org/10.1093/emboj/18.5.1172

Herrera, E., E. Samper, J. Martín-Caballero, J.M. Flores, H.W. Lee, and M.A. Blasco. 1999b. Disease states associated with telomerase deficiency appear earlier in mice with short telomeres. *EMBO J*. 18:2950–2960. https://doi.org/10.1093/emboj/18.11.2950

Higashimoto, Y., Y. Fukuchi, Y. Shimada, K. Ishida, M. Ohata, T. Furuse, C. Shu, S. Teramoto, T. Matsuse, E. Sudo, et al. 1993. The effects of aging on the function of alveolar macrophages in mice. *Mech. Ageing Dev*. 69: 207–217. https://doi.org/10.1016/0047-6374(93)90024-L

Hogan, B.L.M., C.E. Barkauskas, H.A. Chapman, J.A. Epstein, R. Jain, C.C.W. Hsia, L. Niklason, E. Calle, A. Le, S.H. Randell, et al. 2014. Repair and regeneration of the respiratory system: complexity, plasticity, and mechanisms of lung stem cell function. *Cell Stem Cell*. 15:123–138. https://doi.org/10.1016/j.stem.2014.07.012

Hou, J., J. Shi, L. Chen, Z. Lv, X. Chen, H. Cao, Z. Xiang, and X. Han. 2018. M2 macrophages promote myofibroblast differentiation of LR-MSCs and are associated with pulmonary fibrogenesis. *Cell Commun. Signal*. 16:89. https://doi.org/10.1186/s12964-018-0300-8

Hunninghake, G.M.. 2014. A new hope for idiopathic pulmonary fibrosis. *N. Engl. J. Med*. 370:2142–2143. https://doi.org/10.1056/NEJMe1403448

Hussell, T., and T.J. Bell. 2014. Alveolar macrophages: plasticity in a tissue-specific context. *Nat. Rev. Immunol*. 14:81–93. https://doi.org/10.1038/nri3600

Jakubzick, C., E.S. Choi, B.H. Joshi, M.P. Keane, S.L. Kunkel, R.K. Puri, and C.M. Hogaboam. 2003. Therapeutic attenuation of pulmonary fibrosis via targeting of IL-4- and IL-13-responsive cells. *J. Immunol*. 171: 2684–2693. https://doi.org/10.4049/jimmunol.171.5.2684

Karimi-Shah, B.A., and B.A. Chowdhury. 2015. Forced vital capacity in idiopathic pulmonary fibrosis--FDA review of pirfenidone and nintedanib. *N. Engl. J. Med*. 372:1189–1191. https://doi.org/10.1056/NEJMp1500526

King, T.E., Jr., W.Z. Bradford, S. Castro-Bernardini, E.A. Fagan, I. Glaspole, M.K. Glassberg, E. Gorina, P.M. Hopkins, D. Kardatzke, L. Lancaster, et al; ASCEND Study Group. 2014. A phase 3 trial of pirfenidone in patients with idiopathic pulmonary fibrosis. *N. Engl. J. Med*. 370: 2083–2092. https://doi.org/10.1056/NEJMoa1402582

Korfei, M., D. von der Beck, I. Henneke, P. Markart, C. Ruppert, P. Mahavadi, B. Ghanim, W. Klepetko, L. Fink, S. Meiners, et al. 2013. Comparative proteome analysis of lung tissue from patients with idiopathic pulmonary fibrosis (IPF), non-specific interstitial pneumonia (NSIP) and organ donors. *J. Proteomics*. 85:109–128. https://doi.org/10.1016/j.jprot.2013.04.033

Kotton, D.N., and E.E. Morrisey. 2014. Lung regeneration: mechanisms, applications and emerging stem cell populations. *Nat. Med*. 20:822–832. https://doi.org/10.1038/nm.3642

Kuilman, T., C. Michaloglou, L.C.W. Vredeveld, S. Douma, R. van Doorn, C.J. Desmet, L.A. Aarden, W.J. Mooi, and D.S. Peeper. 2008. Oncogene-induced senescence relayed by an interleukin-dependent inflammatory network. *Cell*. 133:1019–1031. https://doi.org/10.1016/j.cell.2008.03.039

Lee, J., R. Reddy, L. Barsky, J. Scholes, H. Chen, W. Shi, and B. Driscoll. 2009. Lung alveolar integrity is compromised by telomere shortening in telomerase-null mice. *Am. J. Physiol. Lung Cell. Mol. Physiol*. 296:L57–L70. https://doi.org/10.1152/ajplung.90411.2008

Ley, B., and H.R. Collard. 2013. Epidemiology of idiopathic pulmonary fibrosis. *Clin. Epidemiol*. 5:483–492. https://doi.org/10.2147/CLEP.S54815

Liu, Y., B.E. Snow, M.P. Hande, D. Yeung, N.J. Erdmann, A. Wakeham, A. Itie, D.P. Siderovski, P.M. Lansdorp, M.O. Robinson, et al. 2000. The telomerase reverse transcriptase is limiting and necessary for telomerase function in vivo. *Curr. Biol*. 10:1459–1462. https://doi.org/10.1016/S0960-9822(00)00805-8

Liu, D., M.S. O'Connor, J. Qin, and Z. Songyang. 2004. Telosome, a mammalian telomere-associated complex formed by multiple telomeric proteins. *J. Biol. Chem*. 279:51338–51342. https://doi.org/10.1074/jbc.M409293200

Liu, T., M.J. Chung, M. Ullenbruch, H. Yu, H. Jin, B. Hu, Y.Y. Choi, F. Ishikawa, and S.H. Phan. 2007. Telomerase activity is required for bleomycin-induced pulmonary fibrosis in mice. *J. Clin. Invest*. 117:3800–3809. https://doi.org/10.1172/JCI32369

Liu, Y.Y., Y. Shi, Y. Liu, X.H. Pan, and K.X. Zhang. 2018. Telomere shortening activates TGF-β/Smads signaling in lungs and enhances both lipopolysaccharide and bleomycin-induced pulmonary fibrosis. *Acta Pharmacol. Sin*. 39:1735–1745. https://doi.org/10.1038/s41401-018-0007-9

Liu, G., H. Zhai, T. Zhang, S. Li, N. Li, J. Chen, M. Gu, Z. Qin, and X. Liu. 2019. New therapeutic strategies for IPF: Based on the "phagocytosis-secretion-immunization" network regulation mechanism of pulmonary macrophages. *Biomed. Pharmacother*. 118. 109230. https://doi.org/10.1016/j.biopha.2019.109230

López-Otín, C., M.A. Blasco, L. Partridge, M. Serrano, and G. Kroemer. 2013. The hallmarks of aging. *Cell*. 153:1194–1217. https://doi.org/10.1016/j.cell.2013.05.039

Lopez-Rodriguez, E., C. Boden, M. Echaide, J. Perez-Gil, M. Kolb, J. Gauldie, U.A. Maus, M. Ochs, and L. Knudsen. 2016. Surfactant dysfunction during overexpression of TGF-β1 precedes profibrotic lung remodeling in vivo. *Am. J. Physiol. Lung Cell. Mol. Physiol*. 310:L1260–L1271. https://doi.org/10.1152/ajplung.00065.2016

Lowery, E.M., A.L. Brubaker, E. Kuhlmann, and E.J. Kovacs. 2013. The aging lung. *Clin. Interv. Aging*. 8:1489–1496. https://doi.org/10.2147/CIA.S51152

Mahavadi, P., M. Korfei, I. Henneke, G. Liebisch, G. Schmitz, B.R. Gochuico, P. Markart, S. Bellusci, W. Seeger, C. Ruppert, et al. 2010. Epithelial stress and apoptosis underlie Hermansky-Pudlak syndrome-associated interstitial pneumonia. *Am. J. Respir. Crit. Care Med*. 182:207–219. https://doi.org/10.1164/rccm.200909-1414OC

Martínez, P., and M.A. Blasco. 2011. Telomeric and extra-telomeric roles for telomerase and the telomere-binding proteins. *Nat. Rev. Cancer*. 11:161–176. https://doi.org/10.1038/nrc3025

Martinez, F.J., H.R. Collard, A. Pardo, G. Raghu, L. Richeldi, M. Selman, J.J. Swigris, H. Taniguchi, and A.U. Wells. 2017. Idiopathic pulmonary fibrosis. *Nat. Rev. Dis. Primers*. 3:17074. https://doi.org/10.1038/nrdp.2017.74

Matsushita, T., S. Elliger, C. Elliger, G. Podsakoff, L. Villarreal, G.J. Kurtzman, Y. Iwaki, and P. Colosi. 1998. Adeno-associated virus vectors can be efficiently produced without helper virus. *Gene Ther*. 5:938–945. https://doi.org/10.1038/sj.gt.3300680

Meiners, S., O. Eickelberg, and M. Königshoff. 2015. Hallmarks of the ageing lung. *Eur. Respir. J*. 45:807–827. https://doi.org/10.1183/09031936.00186914

Mosteiro, L., C. Pantoja, N. Alcazar, R.M. Marión, D. Chondronasiou, M. Rovira, P.J. Fernandez-Marcos, M. Muñoz-Martin, C. Blanco-Aparicio, J. Pastor, et al. 2016. Tissue damage and senescence provide critical signals for cellular reprogramming in vivo. *Science*. 354. aaf4445. https://doi.org/10.1126/science.aaf4445

Muñoz-Lorente, M.A., P. Martínez, Á. Tejera, K. Whittemore, A.C. Moisés-Silva, F. Bosch, and M.A. Blasco. 2018. AAV9-mediated telomerase activation does not accelerate tumorigenesis in the context of oncogenic K-Ras-induced lung cancer. *PLoS Genet*. 14. e1007562. https://doi.org/10.1371/journal.pgen.1007562

Olovnikov, A.M.. 1973. A theory of marginotomy. The incomplete copying of template margin in enzymic synthesis of polynucleotides and biological significance of the phenomenon. *J. Theor. Biol*. 41:181–190. https://doi.org/10.1016/0022-5193(73)90198-7

Pardo, A., and M. Selman. 2017. Fibroblast Senescence and Apoptosis. *Ajrcmb*. 56:145–146.

Parikh, P., S. Wicher, K. Khandalavala, C.M. Pabelick, R.D. Britt, Jr., and Y.S. Prakash. 2019. Cellular senescence in the lung across the age spectrum. *Am. J. Physiol. Lung Cell. Mol. Physiol*. 316:L826–L842. https://doi.org/10.1152/ajplung.00424.2018

Plantier, L., B. Crestani, S.E. Wert, M. Dehoux, B. Zweytick, A. Guenther, and J.A. Whitsett. 2011. Ectopic respiratory epithelial cell differentiation in bronchiolised distal airspaces in idiopathic pulmonary fibrosis. *Thorax*. 66:651–657. https://doi.org/10.1136/thx.2010.151555

Povedano, J.M., P. Martinez, J.M. Flores, F. Mulero, and M.A. Blasco. 2015. Mice with Pulmonary Fibrosis Driven by Telomere Dysfunction. *Cell Rep*. 12:286–299. https://doi.org/10.1016/j.celrep.2015.06.028

Povedano, J.M., P. Martinez, R. Serrano, Á. Tejera, G. Gómez-López, M. Bobadilla, J.M. Flores, F. Bosch, and M.A. Blasco. 2018. Therapeutic effects of telomerase in mice with pulmonary fibrosis induced by damage to the lungs and short telomeres. *eLife*. 7. e31299. https://doi.org/10.7554/eLife.31299

Raghu, G., H.R. Collard, J.J. Egan, F.J. Martinez, J. Behr, K.K. Brown, T.V. Colby, J.F. Cordier, K.R. Flaherty, J.A. Lasky, et al; ATS/ERS/JRS/ALAT Committee on Idiopathic Pulmonary Fibrosis. 2011. An official ATS/ERS/JRS/ALAT statement: idiopathic pulmonary fibrosis: evidence-based guidelines for diagnosis and management. *Am. J. Respir. Crit. Care Med*. 183:788–824. https://doi.org/10.1164/rccm.2009-040GL

Raghu, G., M. Remy-Jardin, J.L. Myers, L. Richeldi, C.J. Ryerson, D.J. Lederer, J. Behr, V. Cottin, S.K. Danoff, F. Morell, et al; American Thoracic Society, European Respiratory Society, Japanese Respiratory Society, and Latin American Thoracic Society. 2018. Diagnosis of idiopathic pulmonary fibrosis An Official ATS/ERS/JRS/ALAT Clinical practice guideline. *Am. J. Respir. Crit. Care Med*. 198:e44–e68. https://doi.org/10.1164/rccm.201807-1255ST

Rawlins, E.L., T. Okubo, Y. Xue, D.M. Brass, R.L. Auten, H. Hasegawa, F. Wang, and B.L.M. Hogan. 2009. The role of Scgb1a1+ Clara cells in the long-term maintenance and repair of lung airway, but not alveolar, epithelium. *Cell Stem Cell*. 4:525–534. https://doi.org/10.1016/j.stem.2009.04.002

Richeldi, L., H.R. Collard, and M.G. Jones. 2017. Idiopathic pulmonary fibrosis. *Lancet*. 389:1941–1952. https://doi.org/10.1016/S0140-6736(17)30866-8

Rock, J.R., C.E. Barkauskas, M.J. Cronce, Y. Xue, J.R. Harris, J. Liang, P.W. Noble, and B.L.M. Hogan. 2011. Multiple stromal populations contribute to pulmonary fibrosis without evidence for epithelial to mesenchymal transition. *Proc. Natl. Acad. Sci. USA*. 108:E1475–E1483. https://doi.org/10.1073/pnas.1117988108

Samper, E., J.M. Flores, and M.A. Blasco. 2001. Restoration of telomerase activity rescues chromosomal instability and premature aging in Terc−/− mice with short telomeres. *EMBO Rep*. 2:800–807. https://doi.org/10.1093/embo-reports/kve174

Schürch, D., O.L. Ospina, A. Cruz, and J. Pérez-Gil. 2010. Combined and independent action of proteins SP-B and SP-C in the surface behavior and mechanical stability of pulmonary surfactant films. *Biophys. J*. 99:3290–3299. https://doi.org/10.1016/j.bpj.2010.09.039

Selman, M., and A. Pardo. 2014. Revealing the pathogenic and aging-related mechanisms of the enigmatic idiopathic pulmonary fibrosis. an integral model. *Am. J. Respir. Crit. Care Med*. 189:1161–1172. https://doi.org/10.1164/rccm.201312-2221PP

Sharpless, N.E., and R.A. DePinho. 2007. How stem cells age and why this makes us grow old. *Nat. Rev. Mol. Cell Biol*. 8:703–713. https://doi.org/10.1038/nrm2241

Snetselaar, R., C.H.M. van Moorsel, K.M. Kazemier, J.J. van der Vis, P. Zanen, M.F.M. van Oosterhout, and J.C. Grutters. 2015. Telomere length in interstitial lung diseases. *Chest*. 148:1011–1018. https://doi.org/10.1378/chest.14-3078

Somogyi, V., N. Chaudhuri, S.E. Torrisi, N. Kahn, V. Müller, and M. Kreuter. 2019. The therapy of idiopathic pulmonary fibrosis: what is next? *Eur. Respir. Rev*. 28. 190021. https://doi.org/10.1183/16000617.0021-2019

Spagnolo, P., T.M. Maher, and L. Richeldi. 2015. Idiopathic pulmonary fibrosis: Recent advances on pharmacological therapy. *Pharmacol. Ther*. 152:18–27. https://doi.org/10.1016/j.pharmthera.2015.04.005

Stanley, S.E., J.J.L. Chen, J.D. Podlevsky, J.K. Alder, N.N. Hansel, R.A. Mathias, X. Qi, N.M. Rafaels, R.A. Wise, E.K. Silverman, et al. 2015. Telomerase mutations in smokers with severe emphysema. *J. Clin. Invest*. 125:563–570. https://doi.org/10.1172/JCI78554

Sun, L., M.C. Louie, K.M. Vannella, C.A. Wilke, A.M. LeVine, B.B. Moore, and T.P. Shanley. 2011. New concepts of IL-10-induced lung fibrosis: fibrocyte recruitment and M2 activation in a CCL2/CCR2 axis. *Am.*

J. Physiol. Lung Cell. Mol. Physiol. 300:L341–L353. https://doi.org/10.1152/ajplung.00122.2010

Takai, H., A. Smogorzewska, and T. de Lange. 2003. DNA damage foci at dysfunctional telomeres. *Curr. Biol.* 13:1549–1556. https://doi.org/10.1016/S0960-9822(03)00542-6

Tompkins, D.H., V. Besnard, A.W. Lange, S.E. Wert, A.R. Keiser, A.N. Smith, R. Lang, and J.A. Whitsett. 2009. Sox2 is required for maintenance and differentiation of bronchiolar Clara, ciliated, and goblet cells. *PLoS One.* 4. e8248. https://doi.org/10.1371/journal.pone.0008248

Tsakiri, K.D., J.T. Cronkhite, P.J. Kuan, C. Xing, G. Raghu, J.C. Weissler, R.L. Rosenblatt, J.W. Shay, and C.K. Garcia. 2007. Adult-onset pulmonary fibrosis caused by mutations in telomerase. *Proc. Natl. Acad. Sci. USA.* 104:7552–7557. https://doi.org/10.1073/pnas.0701009104

Tsang, A.R., H.D.M. Wyatt, N.S.Y. Ting, and T.L. Beattie. 2012. hTERT mutations associated with idiopathic pulmonary fibrosis affect telomerase activity, telomere length, and cell growth by distinct mechanisms. *Aging Cell.* 11:482–490. https://doi.org/10.1111/j.1474-9726.2012.00810.x

Watson, J.D.. 1972. Origin of concatemeric T7 DNA. *Nat. New Biol.* 239:197–201. https://doi.org/10.1038/newbio239197a0

Wong, C.K., C.A. Smith, K. Sakamoto, N. Kaminski, J.L. Koff, and D.R. Goldstein. 2017. Aging Impairs Alveolar Macrophage Phagocytosis and Increases Influenza-Induced Mortality in Mice. *J. Immunol.* 199:1060–1068. https://doi.org/10.4049/jimmunol.1700397

Zhang, L., Y. Wang, G. Wu, W. Xiong, W. Gu, and C.Y. Wang. 2018. Macrophages: friend or foe in idiopathic pulmonary fibrosis? *Respir. Res.* 19:170. https://doi.org/10.1186/s12931-018-0864-2

Supplemental material

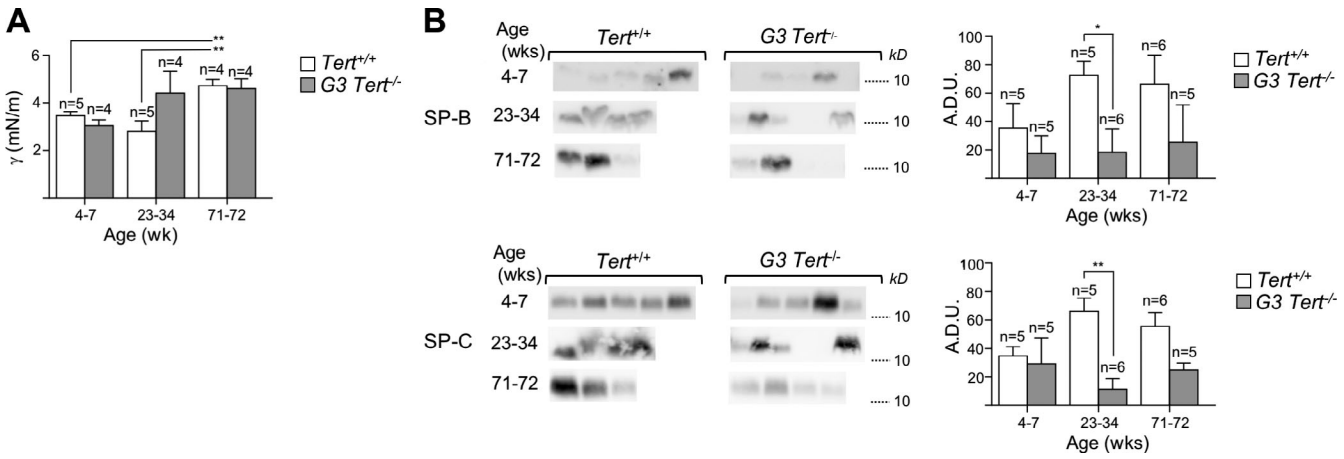

Figure S1. **Physiological aging leads to impaired surfactant activity in wild-type mice, and this is anticipated in telomerase-deficient mice.** Interfacial film stability and WB of hydrophobic surfactant proteins from *Tert*$^{+/+}$ and *G3 Tert*$^{-/-}$ mice with increasing weeks of age. **(A)** Surface tension obtained after hitting five-times-compressed surfactant membranes to test their stability. **(B)** SP-B and SP-C bands obtained by performing WB analysis in reducing conditions, loading the same amount of PC for each sample. Densitometry analysis was performed using as reference the most intense band among the samples tested within each run. White bars represent *Tert*$^{+/+}$ mice. Gray bars represent *G3 Tert*$^{-/-}$ mice. Data are expressed as mean ± SEM (n = 4–6 animals per group). *, P < 0.05; **, P < 0.01 between different ages for each condition using one-way ANOVA with post hoc Dunn–Sidak multiple comparison test or between different conditions within the same age following a Shapiro–Wilk normality test, two-sample unpaired t test, or Mann–Whitney test when appropriate. γ, surface tension; A.D.U., arbitrary densitometry units.

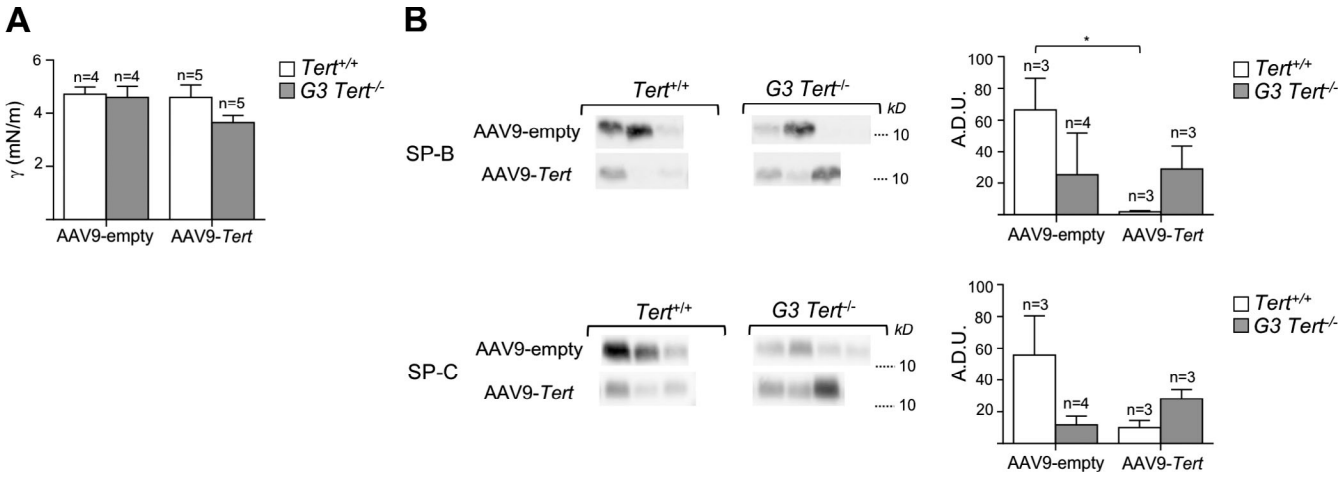

Figure S2. **Telomerase gene therapy prevents age-related worsening in surfactant activity in wild-type and telomerase-deficient mice.** Membrane stability and WB of hydrophobic surfactant proteins from 71–72-wk-old *Tert*$^{+/+}$ and *G3 Tert*$^{-/-}$ mice treated with AAV9-empty or AAV9-*Tert*. **(A)** Surface tension obtained after hitting five-times-compressed surfactant membranes to test their stability. **(B)** SP-B and SP-C bands obtained by performing WB analysis in reducing conditions, loading the same amount of PC for each sample. Densitometry analysis was performed using as reference the most intense band among the samples tested within each run. White bars represent *Tert*$^{+/+}$ mice. Gray bars represent *G3 Tert*$^{-/-}$ mice. Data are expressed as mean ± SEM (n = 3–5 animals per group). *, P < 0.05 between different conditions following a Shapiro–Wilk normality test, two-sample unpaired t test, or Mann–Whitney test when appropriate. γ, surface tension; A.D.U., arbitrary densitometry units.